Hindawi
International Journal of Aerospace Engineering
Volume 2024, Article ID 6636084, 20 pages
https://doi.org/10.1155/2024/6636084

Research Article

Mechanism and Application of Attitude and Orbit Coupling Dynamics for Spacecraft Proximity Relative Motion

An Hao,[1] Li Jin,[1] Wang Tianzhe,[2] Zang Jie,[2] Zhang Xianliang,[3] and Hao Yong[1]

[1]*College of Intelligent Systems Science and Engineering, Harbin Engineering University, Harbin 150001, China*
[2]*China Academy of Space Technology, Beijing 100081, China*
[3]*School of Mathematics and Statistics, Taishan University, Taian 271021, China*

Correspondence should be addressed to Hao Yong; haoyong@hrbeu.edu.cn

Received 19 July 2023; Revised 20 January 2024; Accepted 26 March 2024; Published 6 May 2024

Academic Editor: Chuang Liu

This paper analyzes the root causes of attitude-orbit coupling effects of spacecraft proximity relative motion in space precision collaborative tasks from three aspects: mathematical representation, physical definition, and engineering applications. At first, taking mathematical representation as the context, spacecraft proximity relative motion representations such as particle relative dynamic model, extended particle relative dynamic model, and dual-spiral-based relative dynamic model are investigated in detail. On this basis, the mechanism of attitude-orbit coupling effects originating from different mathematical representations is further investigated. Second, spiral theory–based attitude-orbit coupling relative dynamics is developed. The innovation of this work is extending the dual number representation from rigid body to flexible body, which makes it possible to describe the proximity relative motion between two rigid-flexible coupling spacecraft. Third, the application value of attitude-orbit coupling relative dynamic model in precision collaborative mission such as precision formation, rendezvous and docking, space manipulation, and on-orbit assembly is provided. Finally, simulation results verify the engineering significance of the attitude-orbit coupling relative dynamic model.

Keywords: attitude-orbit coupling; relative dynamics; spacecraft proximity relative motion; spiral theory

1. Introduction

In the research of spacecraft proximity collaborative tasks, such as rendezvous and docking, precision formation, space manipulation, and on-orbit assembly, many scholars have proposed the necessity of attitude-orbit coupling modeling [1–5]. Some scholars have applied the attitude-orbit coupling results to spacecraft guidance, navigation and control (GNC) [6, 7]. Liu et al. [8, 9] proposed various effective attitude-orbit coupling control methods. Obviously, in the field of spacecraft relative dynamics, navigation, and control, attitude-orbit coupling is not a new issue. However, to the author's knowledge, there is no research that has clearly defined attitude-orbit coupling. It is specifically a mathematical problem, a physical phenomenon, or an engineering application problem arising only from practical processes, and there is still controversy.

Due to the unsystematic academic investigations on attitude-orbit coupling, the research results have little guiding significance for engineering applications. In terms of engineering practice, most space missions such as rendezvous and docking [10] and space manipulation technology demonstrations [11] have been successfully deployed on orbit and achieved highly accurate spacecraft cooperative operations without considering the impact of attitude-orbit coupling effect. In the above aerospace engineering tasks, Hill-Clohessy-Wiltshire (HCW) equations [12] are the most widely used relative dynamic model. Obviously, it is not an attitude-orbit coupling relative dynamic model.

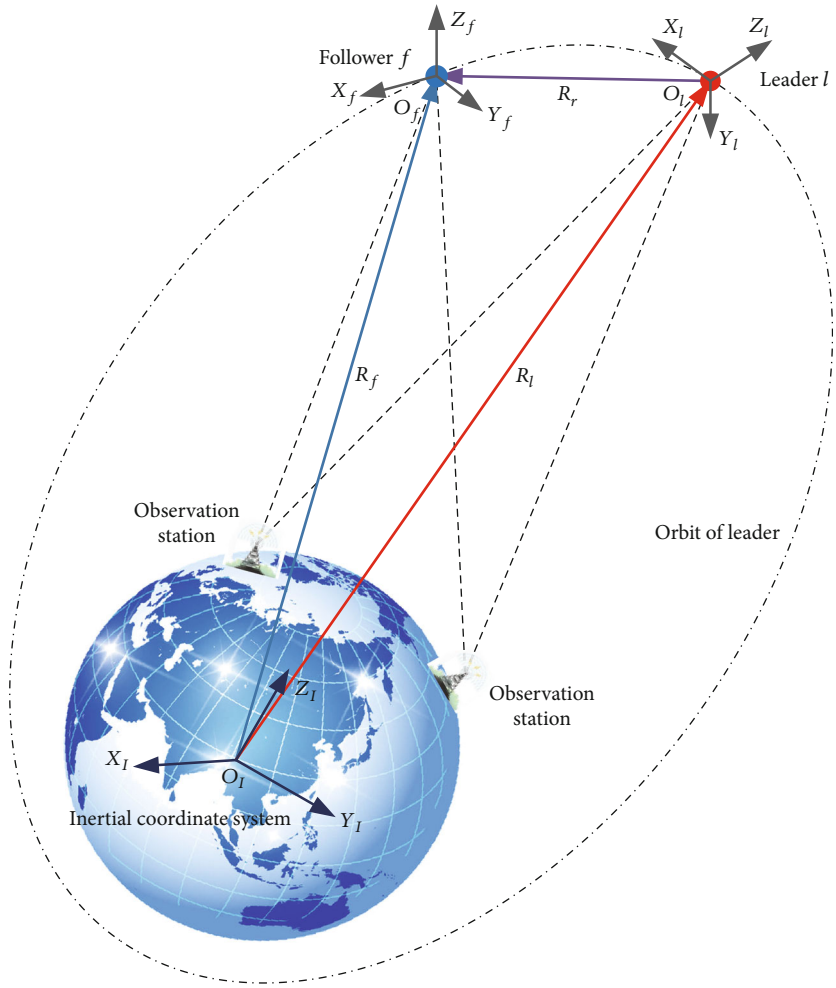

Figure 1: Schematic diagram of the particle model.

The viewpoint proposed in Refs. [1–5] conflicts with the engineering application research in Refs. [10–12], which makes scientific aerospace engineers to wonder whether the research work on attitude-orbit coupling relative dynamic model is necessary, or under what circumstances it is necessary. In addition, in ground experiments, the spacecraft simulator's relative attitude maneuver does not cause relative translational motion [13], which means that the attitude-orbit coupling phenomenon is not explicitly expressed in the physical level, if engineering errors such as inaccurate centroid identification of the spacecraft simulator are ignored.

This paper clarifies, at the first part, the confusion about mechanism and application of attitude-orbit coupling effect and gives a clear definition of attitude-orbit coupling effect. Then, a spiral theory–based attitude-orbit coupling relative dynamic model is developed, which describes the 6-DOF relative motion between spacecraft, whether the spacecraft is a rigid body or a rigid-flexible coupling system, with one equation by using six-dimensional spinor dual vector. Therefore, the spiral theory–based model is known as integrated model [14–16]. Finally, taking spacecraft flying formation as an example, the application value of attitude-orbit coupling relative dynamic model in precision collaborative mission is provided, and simulation results verify the engineering significance of the attitude-orbit coupling relative dynamic model.

2. Mechanism Analysis of Attitude-Orbit Coupling Effects

Aiming at the root cause of the attitude-orbit coupling effects in spacecraft proximity relative motion, taking mathematical representation as the context, the mechanism of attitude-orbit coupling effects originating from different mathematical representation is investigated.

2.1. Particle Model. Since the development of space station rendezvous and docking missions in the 1960s, spacecraft relative dynamic modeling technology has also evolved accordingly. The initial relative dynamic model is known as the particle model, which regarded the relative motion between spacecraft as the relative motion between two points with mass. As shown in Figure 1, the motion of particle f and particle l represents the orbital motion of the follower spacecraft and the leader spacecraft, respectively. $\mathbf{R}_e$, $\dot{\mathbf{R}}_e$, and $\ddot{\mathbf{R}}_e$ denote the relative position, relative velocity,

and relative acceleration between two particles in terms along the inertial system, respectively. If the leader is orbiting on a near circular Earth orbit, the relative dynamics between two spacecraft is [17]

$$m_f \ddot{\mathbf{R}}_e + m_f \mu \left(\frac{\mathbf{R}_l + \mathbf{R}_e}{\|\mathbf{R}_l + \mathbf{R}_e\|^3} - \frac{\mathbf{R}_l}{\|\mathbf{R}_l\|^3} \right) = \mathbf{F}_f. \tag{1}$$

Equation (1) is derived based on Newton's second law, wherein m_f and m_l denote the mass of the follower and leader, respectively, μ is the gravitational constant, and $\mathbf{R}_l$ is the position vector of the leader with respect to the inertial system. $\mathbf{d}_t = \mathbf{d}_f - m_f/m_l \mathbf{d}_l$, where $\mathbf{d}_f$ and $\mathbf{d}_l$ denote the external interference forces acting on the follower and leader, respectively. $\mathbf{F}_t = \mathbf{F}_f - m_f/m_l \mathbf{F}_l$, where $\mathbf{F}_f$ and $\mathbf{F}_l$ denote the control forces acting on the follower and leader, respectively. Note that the external interference forces and control forces are acting on the center of mass (COM) of spacecraft in Equation (1). Based on the particle model, the spacecraft body coordinate system is constructed with the particle as the origin, and the relative attitude dynamic equations between the follower and leader can be expressed as

$$\mathbf{J}_f \dot{\boldsymbol{\omega}}_e + \boldsymbol{\omega}_e \times \mathbf{J}_f \boldsymbol{\omega}_e + \mathbf{d}_f = \boldsymbol{\tau}_f. \tag{2}$$

Equation (2) is derived by using quaternion mathematical representation, wherein $\mathbf{J}_f$ is the moment of inertia of follower, $\boldsymbol{\omega}_e$ denotes the angular velocity tracking error, and $\boldsymbol{\tau}_f$ and $\mathbf{d}_f$ denote the control torque and external interference torque acting on the follower. Note that all vectors in Equations (1) and (2) are expressed with respect to the inertial coordinate system. The relative dynamic equation describing the relative 6-DOF motion between spacecraft can be obtained by combining Equations (1) and (2).

Equations (1) and (2) are derived with respect to the inertial system. This model is used for initial theoretical calculations. If the above equations are expressed in the orbit coordinate system of the leader, the relative dynamic model can be expressed as [18–21]

$$\begin{cases} \ddot{\mathbf{R}}_e = -2\mathbf{n}_l \times \dot{\mathbf{R}}_e - \mathbf{n}_l \times (\mathbf{n}_l \times \mathbf{R}_e) - \dot{\mathbf{n}}_l \times \mathbf{R}_e - \mu \left(\dfrac{\mathbf{R}_l + \mathbf{R}_e}{\|\mathbf{R}_l + \mathbf{R}_e\|^3} - \dfrac{\mathbf{R}_l}{\|\mathbf{R}_l\|^3} \right) + \dfrac{1}{m_f} \mathbf{F}_f \\ \mathbf{J}_f \dot{\boldsymbol{\omega}}_e + \boldsymbol{\omega}_e \times \mathbf{J}_f \boldsymbol{\omega}_e + \mathbf{d}_f = \boldsymbol{\tau}_f \end{cases} \tag{3}$$

where $\mathbf{n}_l$ is angular velocity of the leader orbit. The physical meaning of other parameters is the same as those corresponding to Equations (1) and (2). The difference between Equation (3) and Equations (1) and (2) is that all the vectors are represented in orbit coordinate system of leader. Furthermore, if the leader is orbiting on a circular orbit, the angular velocity of the leader orbit $\mathbf{n}_l$ can be simplified to the constant mean motion, n_l, and Equation (3) can further be expressed in a simple form [10].

$$\begin{cases} \ddot{x} - 2n_l \dot{y} - 3n_l^2 x = \left(\dfrac{1}{m_f} \right) F_{f_x} \\ \ddot{y} + 2n_l \dot{x} = \left(\dfrac{1}{m_f} \right) F_{f_y} \\ \ddot{z} + n_l^2 z = \left(\dfrac{1}{m_f} \right) F_{f_z} \\ \mathbf{J}_f \dot{\boldsymbol{\omega}}_e + \boldsymbol{\omega}_e \times \mathbf{J}_f \boldsymbol{\omega}_e + \mathbf{d}_f = \boldsymbol{\tau}_f \end{cases} \tag{4}$$

where $\mathbf{R}_e = [x \quad y \quad z]^{\mathrm{T}}$ and $\mathbf{F}_f = [F_{f_x} \quad F_{f_y} \quad F_{f_z}]^{\mathrm{T}}$. These above equations of motion are known as the HCW equations. The HCW equations have been used extensively since the 1960s for space cooperative mission modeling [22–24]. The above functions are mainly used for rendezvous and docking missions with orbital hovering and orbital orbiting, as the HCW equation is constructed based on the orbital coordinate system as the reference coordinate system.

Equations (1)–(4) are relative dynamic equations derived from particle model for different engineering applications. Under particle model mathematical framework, the orbital and the attitude motion of spacecraft are independent of each other, and there is no motion projection between the orbital and the attitude motion. Therefore, there is no coupling between the relative attitude and orbit motion between two spacecraft.

2.2. Extended Particle Model. Segal and Gurfil [25] believe that even under particle model mathematical framework, attitude-orbit coupling effect is still a key factor affecting the success of space collaborative tasks, such as rendezvous and docking and spacecraft formation flying (Figure 2). Their argument is that because the size of the spacecraft itself is much smaller than the scale of relative orbital motion, it can be considered as a particle when describing relative motion. However, for space collaborative tasks at ultraclose distances (typically less than 100 m), or for ultraclose stages of certain collaborative tasks, such as the close approximation stage and docking stage of rendezvous and docking mission, the size of the spacecraft can no longer be considered as an absolute small amount compared to the relative motion distance. And the docking point is not actually the COM of the spacecraft, but rather a point on the edge of the spacecraft. Therefore, for the engineering application of above tasks, it is necessary to build the relative dynamic model between the docking points on the spacecraft, instead of the relative dynamic model

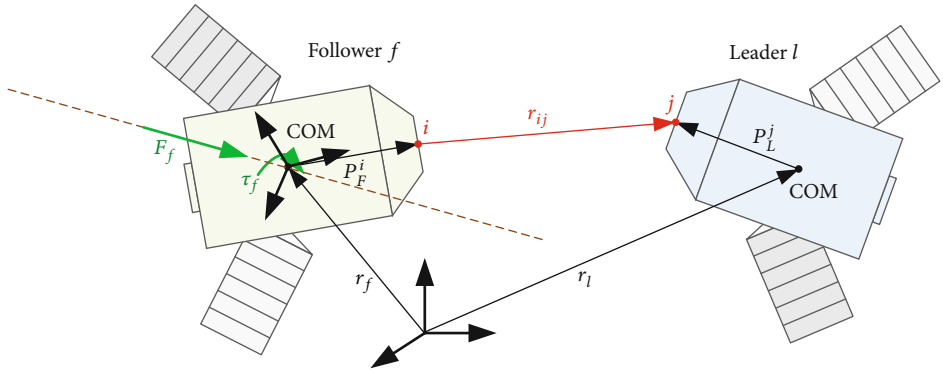

Figure 2: Schematic diagram of the extended particle model.

between COMs of spacecraft, assuming that i and j are the docking points of the follower and leader, respectively. The relative dynamic equations between i and j can be expressed as

$$\begin{cases} \ddot{x}_{ij} - \left[\omega_y\left(\omega_x P_{yf}^i - \omega_y P_{xf}^i\right) + \omega_z\left(\omega_z P_{xf}^i - \omega_x P_{zf}^i\right)\right] - \dot{\omega}_y P_{zf}^i + \dot{\omega}_z P_{yf}^i - 2n\left[\dot{y}_{ij} - \left(\omega_z P_{xf}^i + \omega_x P_{zf}^i\right)\right] + \dot{n}\left(y_{ij} - P_{yf}^i + P_{yl}^j\right) - n^2\left(x_{ij} - P_{xf}^i + P_{xl}^j\right) = \dfrac{-\mu\left(r_l + x_{ij} - P_{xf}^i + P_{xl}^j\right)}{\left[\left(r_l + x_{ij} - P_{xf}^i + P_{xl}^j\right)^2 + \left(y_{ij} - P_{yf}^i + P_{yl}^j\right)^2 + \left(z_{ij} - P_{zf}^i + P_{zl}^j\right)^2\right]^{3/2}} + \dfrac{\mu}{r_l^2} \\ \ddot{y}_{ij} - \left[\omega_z\left(\omega_y P_{zf}^i - \omega_z P_{yf}^i\right) + \omega_x\left(\omega_x P_{yf}^i - \omega_y P_{xf}^i\right)\right] - \dot{\omega}_z P_{xf}^i + \dot{\omega}_x P_{zf}^i + 2n\left[\dot{x}_{ij} - \left(\omega_y P_{zf}^i + \omega_z P_{yf}^i\right)\right] + \dot{n}\left(x_{ij} - P_{xf}^i - P_{xl}^i\right) - n^2\left(y_{ij} - P_{yf}^i + P_{yl}^j\right) = \dfrac{-\mu\left(y_{ij} - P_{yf}^i + P_{yl}^j\right)}{\left[\left(r_l + x_{ij} - P_{xf}^i + P_{xl}^j\right)^2 + \left(y_{ij} - P_{yf}^i + P_{yl}^j\right)^2 + \left(z_{ij} - P_{zf}^i + P_{zl}^j\right)^2\right]^{3/2}} \\ \ddot{z}_{ij} - \left[\omega_x\left(\omega_z P_{xf}^i - \omega_x P_{zf}^i\right) + \omega_y\left(\omega_y P_{zf}^i - \omega_z P_{yf}^i\right)\right] - \dot{\omega}_x P_{yf}^i + \dot{\omega}_y P_{xf}^i = \dfrac{-\mu\left(z_{ij} - P_{zf}^i + P_{zl}^j\right)}{\left[\left(r_l + x_{ij} - P_{xf}^i + P_{xl}^j\right)^2 + \left(y_{ij} - P_{yf}^i + P_{yl}^j\right)^2 + \left(z_{ij} - P_{zf}^i + P_{zl}^j\right)^2\right]^{3/2}} \\ \boldsymbol{J}_f\dot{\boldsymbol{\omega}}_e + \boldsymbol{\omega}_e \times \boldsymbol{J}_f\boldsymbol{\omega}_e + \boldsymbol{d}_f = \boldsymbol{\tau}_f \end{cases} \tag{5}$$

where $\mathbf{r}_{ij} = [x_{ij}, y_{ij}, z_{ij}]^{\mathrm{T}}$ is the relative position vector from docking point i to j, $\mathbf{P}_f^i = [P_{xf}^i, P_{yf}^i, P_{zf}^i]^{\mathrm{T}}$ is the position vector from the COM of the follower to docking point i, $\mathbf{P}_l^j = [P_{xl}^j, P_{yl}^j, P_{zl}^j]^{\mathrm{T}}$ denotes the position vector from the COM of the leader to docking point j, and $\boldsymbol{\omega}_e = [\omega_x, \omega_y, \omega_z]^{\mathrm{T}}$ denotes the angular velocity tracking error.

In Equation (6), it can be found that the relative translational motion is affected by the relative angular velocity $\boldsymbol{\omega}_e$; that is, the spacecraft proximity relative motion is affected by attitude-orbit coupling. Through the simulation of precision formation and rendezvous and docking, Segal and Gurfil conclude that the larger the size of a rigid spacecraft, the stronger the impact of the attitude-orbit coupling effect on the relative motion.

According to the conclusions of the above research, the attitude-orbit coupling effect originates from the relative dynamics between two noncentroid points. It can be inferred that when the particle and COM coincide, the impact of attitude-orbit coupling on relative motion is zero, which is the same as the conclusion drawn in Section 2.1. Obviously, Equation (5) describes a special scenario, not a general equation.

2.3. Spiral Theory–Based Relative Dynamic Model. An attitude-orbit coupling relative dynamic model was provided in 2001 based on the Newton-Euler equations by Pan and Kapila [26], which is also the first publicly published theoretical achievement of attitude-orbit coupling relative dynamics that the authors can find.

$$\begin{cases} \dot{\mathbf{e}}_{v_r} = \dot{\boldsymbol{\rho}}_{v_d} - \boldsymbol{\omega}_e \times \mathbf{e}_{v_r} + \dfrac{1}{m_l}\left(\mathbf{f}_{el} + \mathbf{f}_{dl}\right) - \dfrac{1}{m_l}\mathbf{f}_l - \dfrac{1}{m_f}\left(\mathbf{f}_{ef} + \mathbf{f}_{df}\right) + \dfrac{1}{m_f}\mathbf{f}_f \\ \mathbf{J}_f\dot{\boldsymbol{\omega}}_e + \boldsymbol{\omega}_e \times \mathbf{J}_f\boldsymbol{\omega}_e + \mathbf{d}_f = \boldsymbol{\tau}_f \end{cases} \tag{6}$$

where $\mathbf{e}_{v_r}$ and $\boldsymbol{\rho}_{v_d}$ are the real-time relative orbital velocity and desired relative orbital velocity between the leader and follower, respectively; m_l and m_f are the mass of the leader and follower, respectively; and $\mathbf{f}_{el}$, $\mathbf{f}_{dl}$, and $\mathbf{f}_l$ are the Earth's gravity, external interference force, and control force acting on the leader, respectively. Equation (6) contains element, $\boldsymbol{\omega}_e \times \mathbf{e}_{v_r}$, which shows that the relative rotational motion has an impact on the relative translational motion.

Equation (6) describes the relative dynamics between the COMs of the spacecraft. However, the attitude-orbit

coupling effect occurs. Obviously, this conclusion conflicts with the research conclusions of Equations (1)–(5). It is worth mentioning that Pan and Kapila did not explain the cause of attitude-orbit coupling in Ref. [26] but focused on studying the impact of spacecraft attitude motion caused by gravity gradient torque on relative orbital motion.

In response to the above contradictions, in recent years, Sun et al. [27–29] conducted a detailed study on the attitude-orbit coupling characteristics of relative motion between spacecraft. The attitude-orbit coupling relative dynamics based on spiral theory was obtained.

$$\begin{aligned}\dot{\widehat{\boldsymbol{\omega}}}_e^f = &-\widehat{\mathbf{M}}_f^{-1}\left(\widehat{\boldsymbol{\omega}}_e^f + \widehat{\mathbf{q}}_e^*\widehat{\boldsymbol{\omega}}_l^l\widehat{\mathbf{q}}_e\right)\times\widehat{\mathbf{M}}_f\left(\widehat{\boldsymbol{\omega}}_e^f + \widehat{\mathbf{q}}_e^*\widehat{\boldsymbol{\omega}}_l^l\widehat{\mathbf{q}}_e\right)\\ &+\widehat{\mathbf{M}}_f^{-1}\mathbf{F}_f^f - \widehat{\mathbf{q}}_e^*\dot{\widehat{\boldsymbol{\omega}}}_l^l\widehat{\mathbf{q}}_e + \widehat{\boldsymbol{\omega}}_e^f\times\left(\widehat{\mathbf{q}}_e^*\widehat{\boldsymbol{\omega}}_l^l\widehat{\mathbf{q}}_e\right)\end{aligned} \tag{7}$$

where $\widehat{\boldsymbol{\omega}}_e^f$ and $\mathbf{F}_f^f$ denote the relative dual velocity and dual force acting on the follower, respectively, $\widehat{\mathbf{M}}_f$ is the dual inertia operator of the follower, $\widehat{\mathbf{q}}_e$ is the relative dual quaternion, $\widehat{\mathbf{q}}_e^*$ is the conjugate of $\widehat{\mathbf{q}}_e$, and $\widehat{\boldsymbol{\omega}}_l^l$ is the dual velocity of the leader. Based on the spiral theory, each dual number can represent two separate real vectors with a dual unit ε, which makes the relative dynamic model representation to be in a compact form. According to Ref. [27], it can be found that Equation (7) contains the same coupling element, $\boldsymbol{\omega}_e \times \mathbf{e}_{v_r}$, as Equation (6).

Both Equations (6) and (7) describe the relative motion between the COMs of spacecraft, and the attitude-orbit coupling phenomenon occurs in both equations. Unfortunately, none of the above investigations focused on the mechanism of attitude-orbit coupling phenomenon, but rather on the trajectory offset caused by attitude-orbit coupling effects. It makes engineers wonder what is the root cause of attitude-orbit coupling and what is the difference between the application scenarios of attitude-orbit coupling models and attitude-orbit-independent models.

To clarify this confusion, by analyzing Equations (1)–(4) and Equations (6) and (7), it can be found that Equations (6) and (7) are attitude-orbit coupling relative dynamic model, Equations (1)–(4) are attitude-orbit-independent relative dynamic model, and the above equations all describe the relative motion between COMs of spacecraft. In addition to the mathematical representation, another one of the main differences of above equations is the reference coordinate system. In detail, the reference coordinate system of Equations (1) and (2) is the geocentric inertial coordinate system; the reference coordinate system of Equations (3) and (4) is the orbital coordinate system of leader; the reference coordinate system of Equations (6) and (7) is the body-fixed coordinate system of follower. Based on the above facts, we propose the following conjecture: *attitude-orbit coupling effect between the COMs of spacecraft originates from the selection of reference coordinate system*.

As shown in Figure 3, the position vector of a particle P in the inertial coordinate system is $\mathbf{r}$, the velocity of particle P in the inertial coordinate system is $\mathbf{v}_P^I = d\mathbf{r}/dt$, and the velocity of particle P in the local coordinate system is $\mathbf{v}_P^B = \delta\mathbf{r}/dt$. The relationship between the two can be described as $\mathbf{v}_P^I = \mathbf{v}_{pf} + \delta\mathbf{r}/dt = \boldsymbol{\omega}\times\mathbf{r} + \delta\mathbf{r}/dt$. Specifically, in the description of relative motion of spacecraft, the motion of the COM of leader relative to the COM of the follower is described using the body-fixed coordinate system of the follower as a reference system, thereby introducing relative rotational motion in relative translational motion, resulting in an attitude-orbit coupling characteristic. Therefore, the following inference can be obtained.

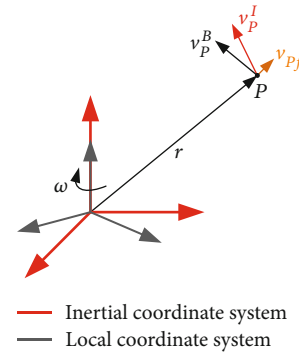

FIGURE 3: Schematic diagram of particle motion in different reference coordinate systems.

Ratiocination Definition 1. Attitude-orbit coupling is the physical phenomena that occur when describing the relative motion between the COMs of spacecraft with respect to a local coordinate system, namely, body-fixed coordinate system.

Ratiocination Definition 2. The dynamic equation also contains attitude-orbit coupling terms even if describing the 6-DOF motion of a single spacecraft with respect to the body-fixed coordinate system. Further, even if the origin of the body-fixed coordinate system coincides with the COM of this spacecraft, the centroid dynamics is also affected by attitude-orbit coupling effect.

2.4. Summary of the Attitude-Orbit Coupling Problems. Based on the above research and analysis, we can conclude that there are two main sources of attitude-orbit coupling effect.

1. The point of motion described by the dynamic equation does not coincide with the point of application of the external force, resulting in additional torque, which leads to attitude-orbit coupling of motion of a single spacecraft, and then, this attitude-orbit coupling effect affects the relative motion between two spacecraft, as shown in Equation (5).

2. Attitude-orbit coupling phenomena occur by using the body-fixed coordinate system as a reference coordinate system to describe relative motion between two spacecraft, as shown in Equations (6) and (7).

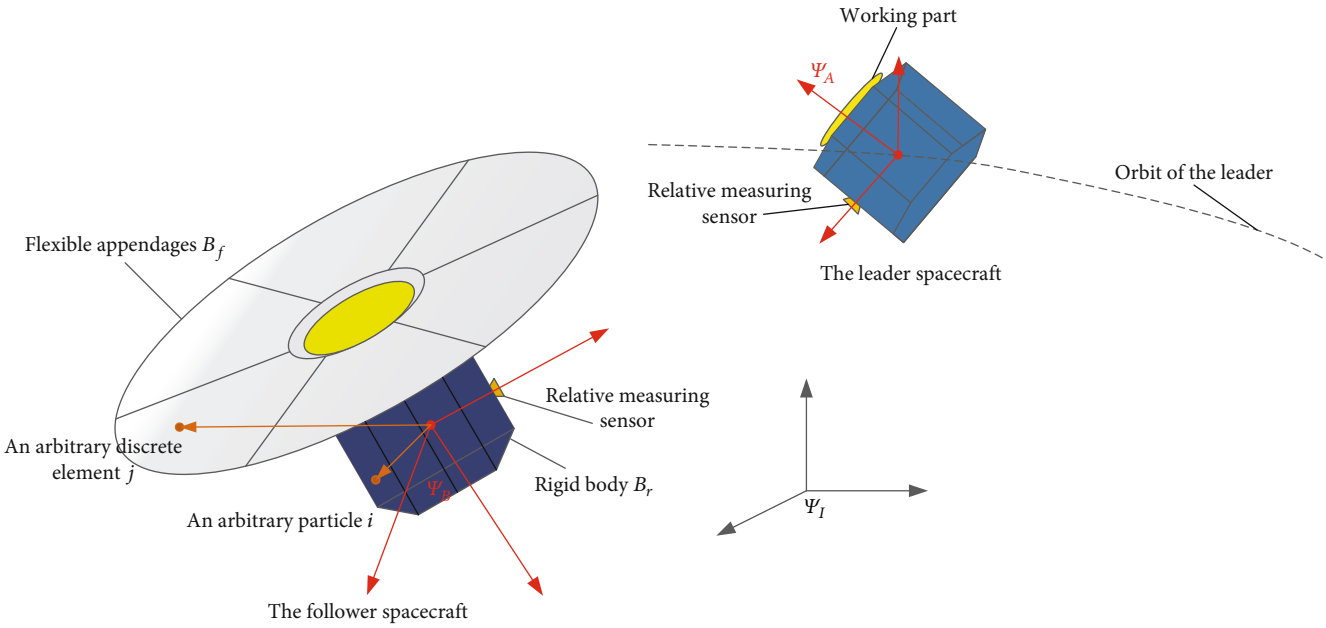

FIGURE 4: Dual vector of a rigid-flexible coupling spacecraft.

Source 1 is a special engineering scenario, and Equation (5) is not a general equation. Therefore, there is little investigation on attitude-orbit coupling relative dynamic modeling caused by source 1. In the following sections of this paper, for attitude-orbit coupling caused by source 2, spiral theory–based attitude-orbit coupling relative dynamics is investigated in detail. The innovation of this work is extending the dual number representation from rigid body to flexible body, which makes it possible to describe the proximity relative motion between two rigid-flexible coupling spacecraft.

3. Spiral Theory–Based Attitude-Orbit Coupling Relative Dynamics

Equation (7) is the spiral theory–based relative dynamics between two rigid spacecraft. Based on Equation (7), the relative dynamic model between two rigid-flexible spacecraft is provided. This model can solve the problem of motion description of spacecraft formation with rigid and flexible spacecraft investigated in Ref. [30].

3.1. Definition of the Coordinate Systems and Equation Assumptions. The mission scenario of this paper is designed to be a spacecraft formation flying task with a rigid spacecraft as the leader and a rigid-flexible coupling spacecraft as the follower. As shown in Figure 4, a simple rigid-flexible coupling spacecraft consists of a rigid base and a flexible appendage. All the coordinate systems are defined in Figure 4, and there are three coordinate systems in this paper.

a. Earth-centered inertial coordinate system $\boldsymbol{\Psi}_I$: the ECI frame is a classic frame for spacecraft dynamic analysis. It has the $+z$-axis pointing at the north pole, the $+x$-axis pointing at the vernal equinox, and $+y$ completing the right-hand set.

b. Body-fixed coordinate system of leader $\boldsymbol{\Psi}_A$: it has the origin locating at the COM of leader, with $+z$-axis pointing at the working part, $+x$ pointing the relative measuring sensor of leader, and $+y$ completing the right-hand set.

c. Body-fixed frame of follower $\boldsymbol{\Psi}_B$: it has the origin locating at the COM of follower, with $+z$-axis pointing at the flexible appendages, $+x$ pointing the relative measuring sensor of follower, and $+y$ completing the right-hand set.

The following notations are employed: $\mathbf{x}^B_{()}$ denotes the components of $\mathbf{x}$ expressed in the body-fixed coordinate system of the follower, and $\mathbf{x}^A_{()}$ denotes the components of $\mathbf{x}$ expressed in the body-fixed coordinate system of the leader.

The derivation of relative dynamics requires the following three conditional assumptions.

Assumption 1. The position of COM and the moment of inertia of the rigid-flexible coupling spacecraft remain unchanged under the vibration of the flexible appendages.

Assumption 2. There is no relative rotation and translation between the flexible appendages and the rigid base; that is, the rigid-flexible spacecraft has a stable configuration.

Assumption 3. The elastic displacement of the flexible appendages is assumed to be small and yields to the linear elasticity theory.

3.2. Attitude-Orbit Coupling Dynamics of the Follower

3.2.1. Dual-Spinor Representation of the Flexible Appendages. Assuming that the angular velocity of $\boldsymbol{\Psi}_B$ relative to $\boldsymbol{\Psi}_I$ is $\boldsymbol{\omega}_B^B$, orbital velocity of the COM of spacecraft B is $\mathbf{v}_B^B$. According to the finite element principle, the rotational velocity and translational velocity of an arbitrary discrete element j of the flexible appendages relative to the COM of the follower can be expressed as

$$\begin{cases} \boldsymbol{\omega}_j^B = \boldsymbol{\omega}_B^B \\ \mathbf{v}_j^B = \mathbf{v}_B^B + \boldsymbol{\omega}_B^B \times \left(\mathbf{r}_{cj}^B + \mathbf{u}_j^B\right) + \dot{\mathbf{u}}_j^B \end{cases} \tag{8}$$

where $\mathbf{r}_{cj}^B$ denotes the position vector from the COM to discrete element j, $\mathbf{u}_j^B$ is the elastic position of j, and $\dot{\mathbf{u}}_j^B$ is the elastic velocity of j.

Let

$$\widehat{\boldsymbol{\omega}}_j^B = \begin{bmatrix} \boldsymbol{\omega}_j^B \\ \mathbf{v}_j^B \end{bmatrix} \tag{9}$$

where $\widehat{\boldsymbol{\omega}}_j^B$ denotes the dual velocity of an arbitrary discrete element j relative to the COM of the follower.

The dual momentum of j with respect to the COM of the follower can be expressed as

$$\widehat{\mathbf{H}}_j^B = \widehat{\mathbf{R}}_{cj}^B \widehat{m}_j \widehat{\boldsymbol{\omega}}_j^B \tag{10}$$

where $\widehat{\mathbf{R}}_{cj}^B = \begin{bmatrix} \mathbf{I}_{3\times3} & 0_{3\times3} \\ [\mathbf{r}_{cj}^B + \mathbf{u}_j^B]^\times & \mathbf{I}_{3\times3} \end{bmatrix}$ is the Hermitian matrix expressed in six-dimensional spinor form (where $\mathbf{I}_{3\times3}$ is the third-order identity matrix) and $\widehat{m}_j = m_j(d/d\varepsilon)$ is the dual mass of j (where m_j is the mass of j). $[\mathbf{r}_{cj}^B + \mathbf{u}_j^B]^\times$ denotes the cross product matrix of $\mathbf{r}_{cj}^B + \mathbf{u}_j^B$.

Introducing Equations (8) and (9) into Equation (10), the dual momentum of j can further be expressed as

$$\begin{aligned} \widehat{\mathbf{H}}_j^B = \widehat{\mathbf{R}}_{cj}^B \widehat{m}_j \widehat{\boldsymbol{\omega}}_j^B = \left[1 + \varepsilon\left(\left[\mathbf{r}_{cj}^B\right]^\times + \left[\mathbf{u}_j^B\right]^\times\right)\right] \left[m_j\left(\mathbf{v}_B^B + \boldsymbol{\omega}_B^B\right.\right. \\ \left.\left. \times \left(\mathbf{r}_{cj}^B + \mathbf{u}_j^B\right) + \dot{\mathbf{u}}_j^B\right)\right]. \end{aligned} \tag{11}$$

According to Assumption 3, the modulus of elastic displacement $\|\mathbf{u}_j^B\|$ is much smaller than $\|\mathbf{r}_{cj}^B\|$, and the elastic displacement $\mathbf{u}_j^B$ can be neglected in the calculation of Equation (11). Subsequently, Equation (11) can be written in the explicit form

$$\begin{aligned} \widehat{\mathbf{H}}_j^B &= \left(1 + \varepsilon\left[\mathbf{r}_{cj}^B\right]^\times\right)\left[m_j\left(\mathbf{v}_B^B + \boldsymbol{\omega}_B^B \times \mathbf{r}_{cj}^B + \dot{\mathbf{u}}_j^B\right)\right] \\ &= m_j \mathbf{v}_B^B + m_j\left[\mathbf{r}_{jc}^B\right]^\times \boldsymbol{\omega}_B^B + m_j \dot{\mathbf{u}}_j^B + \varepsilon m_j\left[\mathbf{r}_{cj}^B\right]^\times \mathbf{v}_B^B \\ &\quad + \varepsilon m_j\left[\mathbf{r}_{cj}^B\right]^\times \left[\mathbf{r}_{jc}^B\right]^\times \boldsymbol{\omega}_B^B + \varepsilon m_j\left[\mathbf{r}_{cj}^B\right]^\times \dot{\mathbf{u}}_j^B \end{aligned} \tag{12}$$

where $[\mathbf{r}_{jc}^B]^\times \boldsymbol{\omega}_B^B = [\boldsymbol{\omega}_B^B]^\times \mathbf{r}_{cj}^B$.

Based on the finite element principle, the dual momentum of the flexible appendages B_f, with respect to the body-fixed coordinate system of follower, is obtained.

$$\widehat{\mathbf{H}}_{B_f}^B = \sum_{j=1}^{N} \widehat{\mathbf{H}}_j^B,\ j = 1, 2, \cdots, N \tag{13}$$

where $\widehat{\mathbf{H}}_{B_f}^B$ denotes the dual momentum of the flexible appendages.

Introducing Equation (12) into Equation (13), the specific expression of dual momentum of the flexible appendages B_f is obtained.

$$\begin{aligned} \widehat{\mathbf{H}}_{B_f}^B &= \sum_{j=1}^{N} m_j \mathbf{v}_B^B + \sum_{j=1}^{N} m_j\left[\mathbf{r}_{jc}^B\right]^\times \boldsymbol{\omega}_B^B + \sum_{j=1}^{N} m_j \dot{\mathbf{u}}_j^B \\ &\quad + \varepsilon \sum_{j=1}^{N} m_j\left[\mathbf{r}_{cj}^B\right]^\times \mathbf{v}_B^B + \varepsilon \sum_{j=1}^{N} m_j\left[\mathbf{r}_{cj}^B\right]^\times \left[\mathbf{r}_{jc}^B\right]^\times \boldsymbol{\omega}_B^B \\ &\quad + \varepsilon \sum_{j=1}^{N} m_j\left[\mathbf{r}_{cj}^B\right]^\times \dot{\mathbf{u}}_j^B. \end{aligned} \tag{14}$$

Let

$$\begin{aligned} m_{B_f} &= \sum_{j=1}^{N} m_j,\ \left[\mathrm{V}_{B_f}\right]^\times = \sum_{j=1}^{N} m_j\left[\mathbf{r}_{cj}^B\right]^\times,\ \left[\mathrm{V}_{B_f}\right]_{\mathrm{V}}^\times \\ &= \sum_{j=1}^{N} m_j\left[\mathbf{r}_{jc}^B\right]^\times,\ \mathbf{J}_{B_f} = \sum_{j=1}^{N} m_j\left[\mathbf{r}_{cj}^B\right]^\times\left[\mathbf{r}_{jc}^B\right]^\times \end{aligned} \tag{15}$$

where m_{B_f} and $\mathbf{J}_{B_f}$ denote the mass and the moment of inertia of the flexible appendages, respectively.

Then, Equation (14) can be further expressed as

$$\begin{aligned} \widehat{\mathbf{H}}_{B_f}^B &= m_{B_f} \mathbf{v}_B^B + \left[\mathrm{V}_{B_f}\right]_{\mathrm{V}}^\times \boldsymbol{\omega}_B^B + \sum_{j=1}^{N} m_j \dot{\mathbf{u}}_j^B + \varepsilon\left[\mathrm{V}_{B_f}\right]^\times \mathbf{v}_B^B \\ &\quad + \varepsilon \mathbf{J}_{B_f} \boldsymbol{\omega}_B^B + \varepsilon \sum_{j=1}^{N} m_j\left[\mathbf{r}_{cj}^B\right]^\times \dot{\mathbf{u}}_j^B. \end{aligned} \tag{16}$$

Having formulated the discrete model of the dual momentum of the flexible body, we proceed from Equation (16) with model transformation

$$\mathbf{u}_j^B = \boldsymbol{\Phi}_j \boldsymbol{\eta},\ \dot{\mathbf{u}}_j^B = \boldsymbol{\Phi}_j \dot{\boldsymbol{\eta}} \tag{17}$$

where $\boldsymbol{\eta} \in \mathbb{R}^{N\times 1}$ (where N is the truncation number) is the modal coordinate matrix of the flexible body and $\boldsymbol{\Phi}_j$ is the matrix of eigenvectors of j.

In addition, let

$$\mathbf{B}_{\text{tran}} = \sum_{j=1}^{N} m_j \boldsymbol{\Phi}_j, \mathbf{B}_{\text{rot}} = \sum_{j=1}^{N} m_j \left[\mathbf{r}_{cj}^{b}\right]^{\times} \boldsymbol{\Phi}_j \tag{18}$$

where $\mathbf{B}_{\text{tran}}$ is the rigid-flexible translational coupling matrix and $\mathbf{B}_{\text{rot}}$ is the rigid-flexible rotational coupling matrix.

Substituting Equations (17) and (18) into Equation (16) and representing Equation (16) in 6-DOF matrix form, we can obtain

$$\widehat{\mathbf{H}}_{B_f}^{B} = \begin{bmatrix} \left[\mathrm{V}_{B_f}\right]_{\mathrm{v}}^{\times} & m_{B_f}\mathbf{I}_{3\times 3} \\ \mathbf{J}_B & \left[\mathrm{V}_{B_f}\right]^{\times} \end{bmatrix} \begin{bmatrix} \boldsymbol{\omega}_B^B \\ \mathbf{v}_B^B \end{bmatrix} + \begin{bmatrix} \mathbf{B}_{tran} & 0_{3\times N} \\ 0_{3\times N} & \mathbf{B}_{rot} \end{bmatrix} \begin{bmatrix} \dot{\boldsymbol{\eta}} \\ \ddot{\boldsymbol{\eta}} \end{bmatrix}. \tag{19}$$

Let

$$\widehat{\mathbf{M}}_{B_f} = \begin{bmatrix} \left[\mathrm{V}_{B_f}\right]_{\mathrm{v}}^{\times} & m_{B_f}\mathbf{I}_{3\times 3} \\ \mathbf{J}_{B_r} & \left[\mathrm{V}_{B_f}\right]^{\times} \end{bmatrix}, \widehat{\mathbf{B}}_{B_f} = \begin{bmatrix} \mathbf{B}_{tran} & 0_{3\times N} \\ 0_{3\times N} & \mathbf{B}_{rot} \end{bmatrix}. \tag{20}$$

Introducing Equation (20) into Equation (19), one can obtain

$$\widehat{\mathbf{H}}_{B_f}^{B} = \widehat{\mathbf{M}}_{B_f} \widehat{\boldsymbol{\omega}}_B^B + \widehat{\mathbf{B}}_{B_f} \dot{\widehat{\boldsymbol{\eta}}} \tag{21}$$

where $\widehat{\mathbf{M}}_{B_f}$ and $\widehat{\mathbf{B}}_{B_f}$ denote the dual inertia operator and dual rigid-flexible coupling operator, respectively. $\dot{\widehat{\boldsymbol{\eta}}} = \begin{bmatrix} \dot{\boldsymbol{\eta}} \\ \ddot{\boldsymbol{\eta}} \end{bmatrix}$ denotes the dual modal coordinates of the flexible appendages. Note that $\widehat{\boldsymbol{\eta}}$ has no physical property, and it is only a dual operator for compact construction.

3.2.2. Dual-Spinor Representation of the Rigid Base. The same mathematical representation is adopted to derive the dual momentum of the rigid base. The rigid base can be equivalent to a system of particles. The attitude and orbital velocity of an arbitrary particle, i, with respect to $\boldsymbol{\Psi}_B$ can be expressed as

$$\begin{cases} \boldsymbol{\omega}_i^B = \boldsymbol{\omega}_B^B \\ \mathbf{v}_i^B = \mathbf{v}_B^B + \boldsymbol{\omega}_B^B \times \mathbf{r}_{ci}^B \end{cases} \tag{22}$$

where $\mathbf{r}_{ci}^B$ is the position vector from the COM of the follower to particle i.

Then, the dual momentum of i with respect to $\boldsymbol{\Psi}_B$ can be expressed as

$$\widehat{\mathbf{H}}_i^B = \widehat{\mathbf{R}}_{ci}^B \widehat{m}_i \widehat{\boldsymbol{\omega}}_i^B \tag{23}$$

where $\widehat{\mathbf{R}}_{ci}^B = \begin{bmatrix} \mathbf{I}_{3\times 3} & 0_{3\times 3} \\ \left[\mathbf{r}_{cj}^B\right]^{\times} & \mathbf{I}_{3\times 3} \end{bmatrix}$, $\widehat{\boldsymbol{\omega}}_i^B = \begin{bmatrix} \boldsymbol{\omega}_i^B \\ \mathbf{v}_i^B \end{bmatrix}$, and $\widehat{m}_i$ is the dual mass of particle i.

Dual momentum of the rigid base is equivalent to the dual momentum of a system of particles, and the dual momentum of a system of particles is a sum of linear dual momentum of each particle.

$$\begin{aligned} \widehat{\boldsymbol{H}}_{B_r}^B &= \sum_{i=1}^{N} \widehat{\boldsymbol{H}}_i^B = \sum_{i=1}^{N} \widehat{\boldsymbol{R}}_{ci}^B \widehat{m}_i \widehat{\boldsymbol{\omega}}_i^B = \sum_{i=1}^{N} m_i \boldsymbol{v}_B^B + \sum_{i=1}^{N} m_i \left[\boldsymbol{r}_{ic}^B\right]^{\times} \boldsymbol{\omega}_B^B \\ &+ \varepsilon \sum_{i=1}^{N} m_i \left[\boldsymbol{r}_{ci}^B\right]^{\times} \boldsymbol{v}_B^B + \varepsilon \sum_{i=1}^{N} \boldsymbol{m}_i \left[\boldsymbol{r}_{ci}^B\right]^{\times} \left[\boldsymbol{r}_{ic}^B\right]^{\times} \boldsymbol{\omega}_B^B = m_{B_r} \boldsymbol{v}_B^B \\ &+ \left[\mathrm{V}_{B_r}\right]_{\mathrm{V}}^{\times} \boldsymbol{\omega}_B^B + \varepsilon \left[\mathrm{V}_{B_r}\right]^{\times} \boldsymbol{v}_B^B + \varepsilon \boldsymbol{J}_{B_r} \boldsymbol{\omega}_B^B \end{aligned} \tag{24}$$

where

$$\begin{aligned} m_{B_r} &= \sum_{i=1}^{N} m_i, \left[\mathrm{V}_{B_i}\right]^{\times} = \sum_{i=1}^{N} m_i \left[\mathbf{r}_{ci}^B\right]^{\times}, \left[\mathrm{V}_{B_r}\right]_{\mathrm{V}}^{\times} \\ &= \sum_{i=1}^{N} m_i \left[\mathbf{r}_{ic}^B\right]^{\times}, \mathbf{J}_{B_r} = \sum_{i=1}^{N} m_i \left[\mathbf{r}_{ci}^B\right]^{\times} \left[\mathbf{r}_{ic}^B\right]^{\times}. \end{aligned} \tag{25}$$

Representing Equation (16) in 6-DOF matrix form, the dual momentum of the rigid base can further be expressed as

$$\widehat{\mathbf{H}}_{B_r}^{B} = \begin{bmatrix} \left[\mathrm{V}_{B_r}\right]_{\mathrm{v}}^{\times} & m_{B_r}\mathbf{I}_{3\times 3} \\ \mathbf{J}_{B_r} & \left[\mathrm{V}_{B_r}\right]^{\times} \end{bmatrix} \begin{bmatrix} \boldsymbol{\omega}_B^B \\ \mathbf{v}_B^B \end{bmatrix}. \tag{26}$$

Let

$$\widehat{\mathbf{M}}_{B_r} = \begin{bmatrix} \left[\mathrm{V}_{B_r}\right]_{\mathrm{v}}^{\times} & m_{B_r}\mathbf{I}_{3\times 3} \\ \mathbf{J}_{B_r} & \left[\mathrm{V}_{B_r}\right]^{\times} \end{bmatrix}. \tag{27}$$

Equation (26) can further be expressed as

$$\widehat{\mathbf{H}}_{B_r}^{B} = \widehat{\mathbf{M}}_{B_r} \widehat{\boldsymbol{\omega}}_B^B. \tag{28}$$

3.2.3. Dual-Spinor Representation of the Dynamics of Rigid-Flexible Coupling Spacecraft. Dual momentum of the rigid-flexible coupling spacecraft can be expressed as the sum of Equations (21) and (28).

$$\widehat{\mathbf{H}}_B^B = \widehat{\mathbf{H}}_{B_f}^B + \widehat{\mathbf{H}}_{B_r}^B = \left(\widehat{\mathbf{M}}_{B_f} + \widehat{\mathbf{M}}_{B_r}\right) \widehat{\boldsymbol{\omega}}_B^B + \widehat{\mathbf{B}}_{B_f} \dot{\widehat{\boldsymbol{\eta}}}. \tag{29}$$

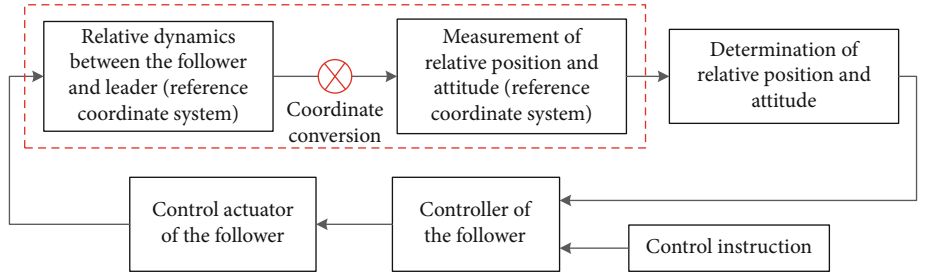

Figure 5: GNC system of the spacecraft in a spacecraft proximity mission.

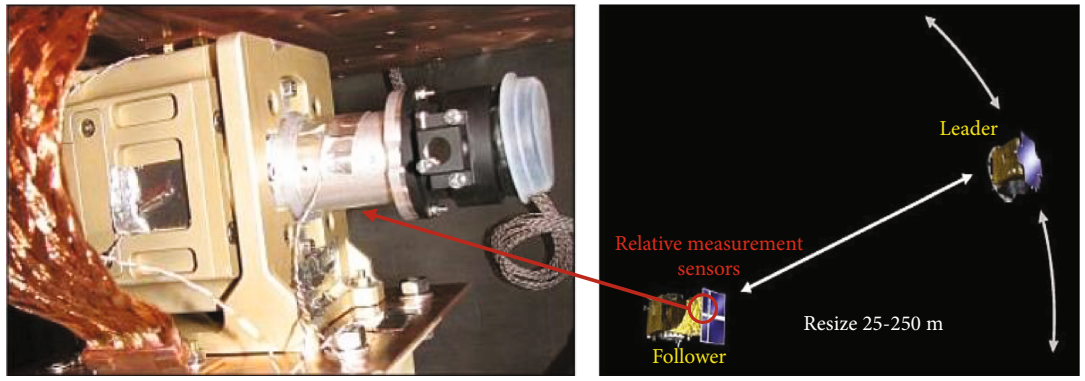

High accuracy metrology sensor based on laser metrology PROBA-3 mission

Figure 6: Measurement device in a spacecraft proximity mission.

In addition, let

$$\widehat{\mathbf{M}}_B = \widehat{\mathbf{M}}_{B_f} + \widehat{\mathbf{M}}_{B_r} = \begin{bmatrix} \left[\mathrm{V}_{B_f}\right]_{\mathrm{v}}^{\times} + \left[\mathrm{V}_{B_r}\right]_{\mathrm{v}}^{\times} & \left(m_{B_f} + m_{B_r}\right)\mathbf{I}_{3\times 3} \\ \mathbf{J}_{B_f} + \mathbf{J}_{B_r} & \left[\mathrm{V}_{B_f}\right]^{\times} + \left[\mathrm{V}_{B_r}\right]^{\times} \end{bmatrix} \tag{30}$$

where $m_B = m_{B_f} + m_{B_r}$ and $\mathbf{J}_B = \mathbf{J}_{B_f} + \mathbf{J}_{B_r}$ denote the mass and moment of inertia of rigid-flexible coupling spacecraft, respectively.

According to the Assumption 1 and Assumption 2, Equation (30) includes mutually canceling terms.

$$\left[\mathrm{V}_{B_f}\right]_{\mathrm{v}}^{\times} + \left[\mathrm{V}_{B_r}\right]_{\mathrm{v}}^{\times} = 0, \left[\mathrm{V}_{B_f}\right]^{\times} + \left[\mathrm{V}_{B_r}\right]^{\times} = 0. \tag{31}$$

The dual momentum of rigid-flexible coupling spacecraft can further be expressed as

$$\widehat{\mathbf{H}}_B^B = \widehat{\mathbf{M}}_B \widehat{\boldsymbol{\omega}}_B^B + \widehat{\mathbf{B}}_{B_f} \dot{\widehat{\boldsymbol{\eta}}} \tag{32}$$

where $\widehat{\mathbf{M}}_B = \begin{bmatrix} 0_{3\times 3} & m_B \mathbf{I}_{3\times 3} \\ \mathbf{J}_B & 0_{3\times 3} \end{bmatrix}$ is the dual inertia operator of the follower.

Xie et al. [29] provided a time derivative rule of dual momentum. Dynamic equation can be derived using along

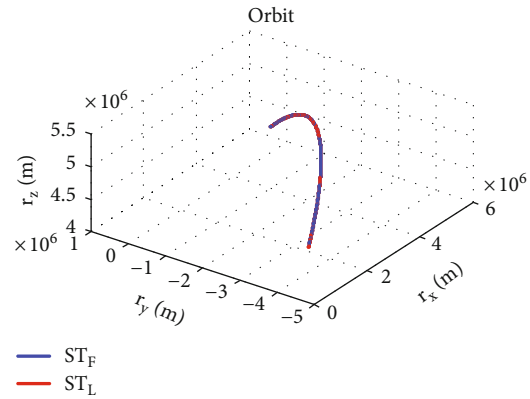

Figure 7: Relative motion trajectory between two spacecraft in inertial frame.

with the time derivative rule of dual momentum

$$\frac{d}{dt}\widehat{\mathbf{H}}_B^B = \frac{\partial}{\partial t}\widehat{\mathbf{H}}_B^B + \widehat{\boldsymbol{\omega}}_B^B \times \widehat{\mathbf{H}}_B^B. \tag{33}$$

Note that Equation (33) can be adopted only when the reference coordinate system of the 6-DOF dynamics is a local coordinate system. That is, the dynamics and relative dynamics based on dual number with Newton-Euler form is derived with respect to the body-fixed coordinate system.

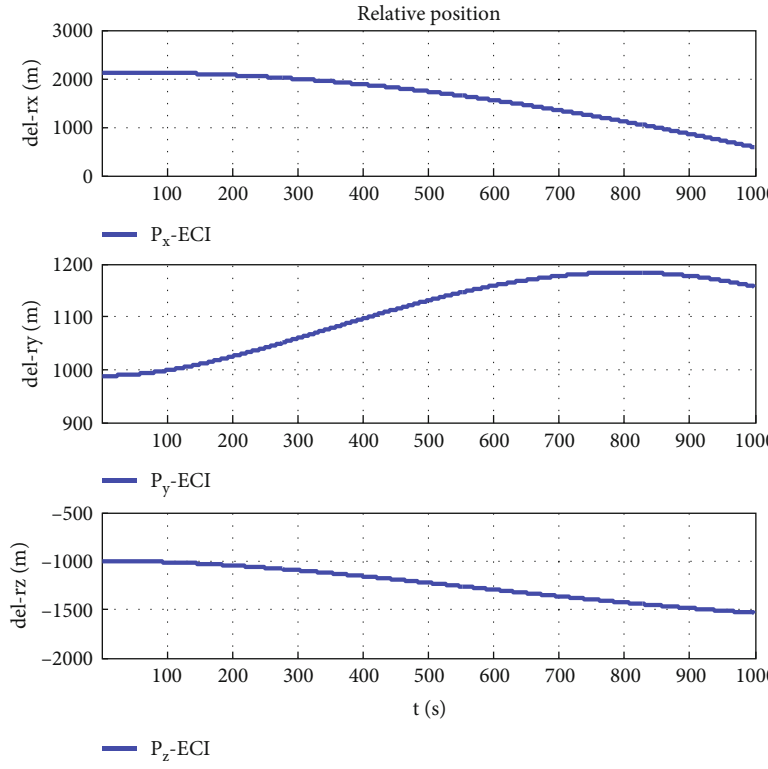

Figure 8: Relative position in inertial frame.

The dynamic equation of a rigid-flexible spacecraft can be obtained by substituting Equation (32) into Equation (33).

$$\mathbf{F}_B^B = \hat{\mathbf{M}}_B \dot{\hat{\boldsymbol{\omega}}}_B^B + \hat{\mathbf{B}}_{B_f} \ddot{\hat{\boldsymbol{\eta}}} + \hat{\boldsymbol{\omega}}_B^B \times \hat{\mathbf{M}}_B \hat{\boldsymbol{\omega}}_B^B + \hat{\boldsymbol{\omega}}_B^B \times \hat{\mathbf{B}}_{B_f} \dot{\hat{\boldsymbol{\eta}}} \tag{34}$$

where $\mathbf{F}_B^B = \begin{bmatrix} \mathbf{F}_B^B \\ \mathbf{T}_B^B \end{bmatrix}$ is the dual forces acting on the COM of the follower.

3.3. Dual-Spinor Representation of Relative Dynamics Between a Rigid-Flexible Spacecraft and a Rigid Spacecraft. According to Ref. [31], the relative kinematic equation between the follower and leader can be expressed as

$$\dot{\hat{\mathbf{q}}}_{BA} = \frac{1}{2} \hat{\mathbf{q}}_{BA} \tilde{\hat{\boldsymbol{\omega}}}_{BA}^B \tag{35}$$

where $\tilde{\hat{\boldsymbol{\omega}}}_{BA}^B = [0 \quad \boldsymbol{\omega}_{BA}^{B\,\mathrm{T}}]^{\mathrm{T}} + \varepsilon [0 \quad \mathbf{v}_{BA}^{B\,\mathrm{T}}]^{\mathrm{T}}$, $\hat{\boldsymbol{\omega}}_{BA}^B = \boldsymbol{\omega}_{BA}^B + \varepsilon \mathbf{v}_{BA}^B$ denotes the dual velocity of the follower relative to the leader, and $\boldsymbol{\omega}_{BA}^B$ and $\mathbf{v}_{BA}^B$ denote the relative angular velocity and relative linear velocity, respectively.

The relative dual velocity $\hat{\boldsymbol{\omega}}_{BA}^B$ can be obtained by the following equation.

$$\hat{\boldsymbol{\omega}}_{BA}^B = \hat{\boldsymbol{\omega}}_B^B - \hat{\boldsymbol{\omega}}_A^B = \hat{\boldsymbol{\omega}}_B^B - E_x \left\{ \hat{\mathbf{q}}_{BA}^* \tilde{\hat{\boldsymbol{\omega}}}_A^A \hat{\mathbf{q}}_{BA} \right\} \tag{36}$$

where $\hat{\boldsymbol{\omega}}_A^B$ and $\hat{\boldsymbol{\omega}}_A^A$ denote the dual velocity of the leader expressed in body-fixed coordinate system of the follower and body-fixed coordinate system of the leader, respectively, and $E_x\{\cdot\}$ is the dimensionality reduction operator, for example, $E_x\{\tilde{\hat{\boldsymbol{\omega}}}_A^A\} = \boldsymbol{\omega}_A^A + \varepsilon \mathbf{v}_A^A$.

Substituting Equation (34) into Equation (36) and taking the first derivative, we obtain a dual-spinor representation of the relative dynamic equation between a rigid-flexible spacecraft and a rigid spacecraft.

$$\begin{aligned} \dot{\hat{\boldsymbol{\omega}}}_{BA}^B &= \dot{\hat{\boldsymbol{\omega}}}_B^B - E_x \left\{ \hat{\mathbf{q}}_{BA}^* \dot{\tilde{\hat{\boldsymbol{\omega}}}}_A^A \hat{\mathbf{q}}_{BA} \right\} + \hat{\boldsymbol{\omega}}_{BA}^B \times E_x \left\{ \hat{\mathbf{q}}_{BA}^* \tilde{\hat{\boldsymbol{\omega}}}_A^A \hat{\mathbf{q}}_{BA} \right\} \\ &= \hat{\boldsymbol{M}}_B^{-1} \boldsymbol{F}_B^B - \hat{\boldsymbol{M}}_B^{-1} \hat{\boldsymbol{B}}_{B_f} \ddot{\hat{\boldsymbol{\eta}}} - \hat{\boldsymbol{M}}_B^{-1} \hat{\boldsymbol{\omega}}_B^B \times \left(\hat{\boldsymbol{M}}_B \hat{\boldsymbol{\omega}}_B^B + \hat{\boldsymbol{B}}_{B_f} \dot{\hat{\boldsymbol{\eta}}} \right) \\ &\quad - E_x \left\{ \hat{\mathbf{q}}_{BA}^* \dot{\tilde{\hat{\boldsymbol{\omega}}}}_A^A \hat{\mathbf{q}}_{BA} \right\} + \hat{\boldsymbol{\omega}}_{BA}^B \times E_x \left\{ \hat{\mathbf{q}}_{BA}^* \tilde{\hat{\boldsymbol{\omega}}}_A^A \hat{\mathbf{q}}_{BA} \right\}. \end{aligned} \tag{37}$$

The modal coordinates $\boldsymbol{\eta}$, $\dot{\boldsymbol{\eta}}$, and $\ddot{\boldsymbol{\eta}}$ can be obtained through the vibration equation [5]

$$\ddot{\boldsymbol{\eta}} + 2\xi \Lambda \dot{\boldsymbol{\eta}} + \Lambda^2 \boldsymbol{\eta} + \mathbf{B}_{tran}^{\mathrm{T}} \dot{\mathbf{v}}_{BA}^B + \mathbf{B}_{rot}^{\mathrm{T}} \dot{\boldsymbol{\omega}}_{BA}^B = 0 \tag{38}$$

where Λ denotes the vector of natural angular frequencies and ξ denotes the vector of modal damping factors.

By combining Equations (35), (37), and (38), the relative kinematic and dynamic equations between two flexible spacecraft are obtained. It is worth noting that the dynamic model developed in Equation (27) is applicable to both circular and elliptical orbits.

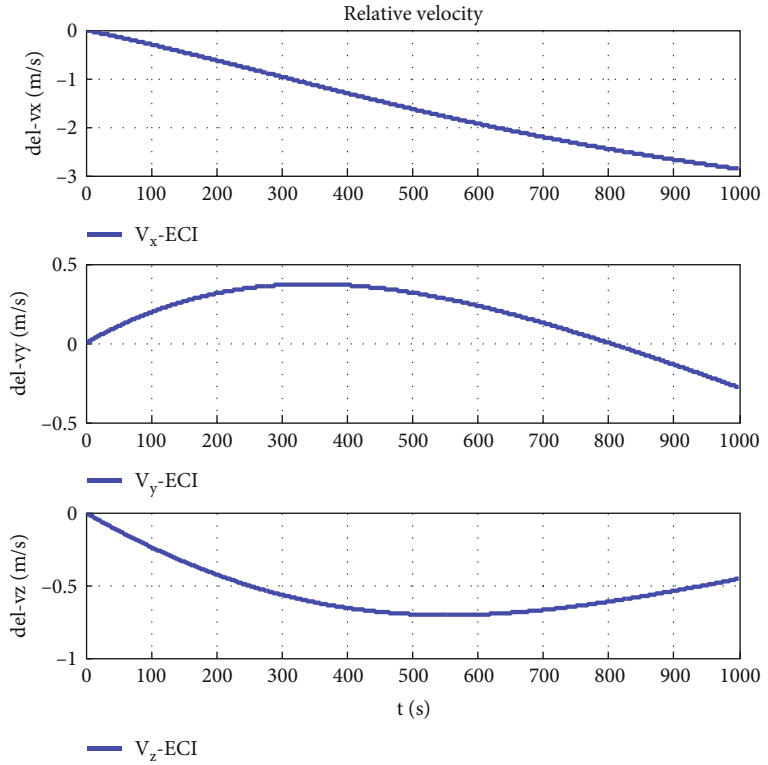

Figure 9: Relative velocity in inertial frame.

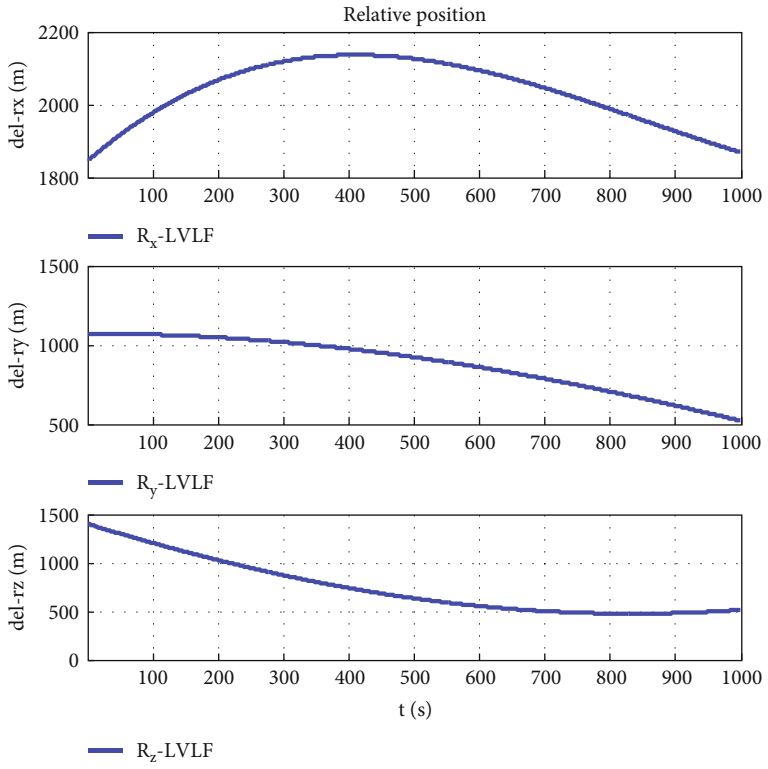

Figure 10: Relative position when navigation error is zero.

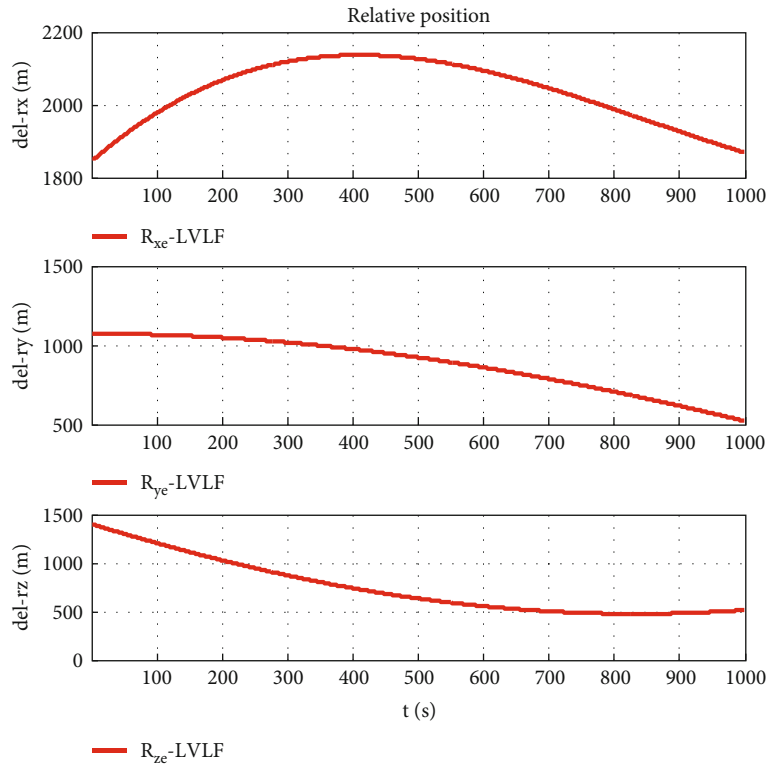

Figure 11: Relative position when navigation error is $\Delta\mathbf{r}$.

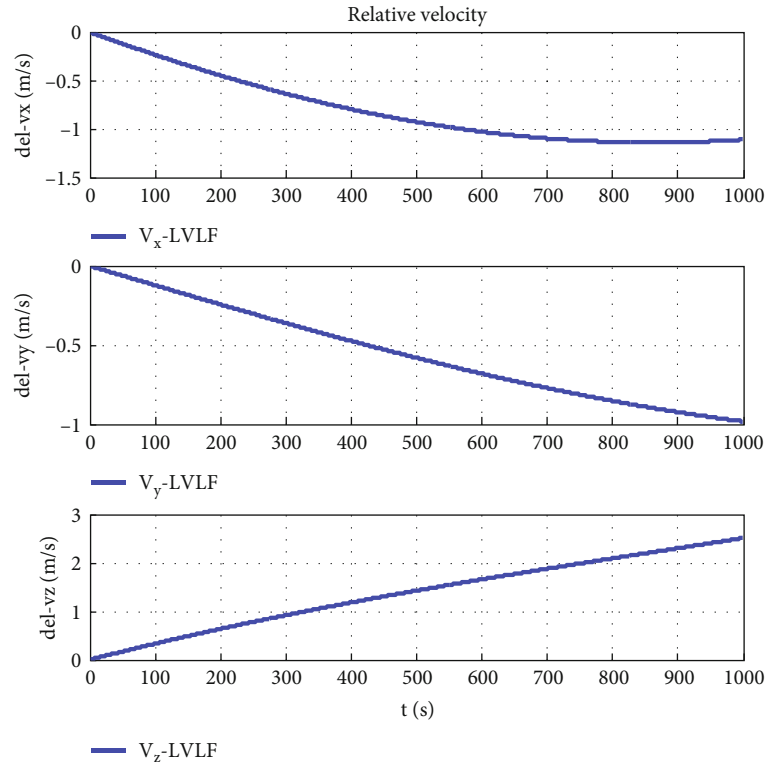

Figure 12: Relative velocity when navigation error is zero.

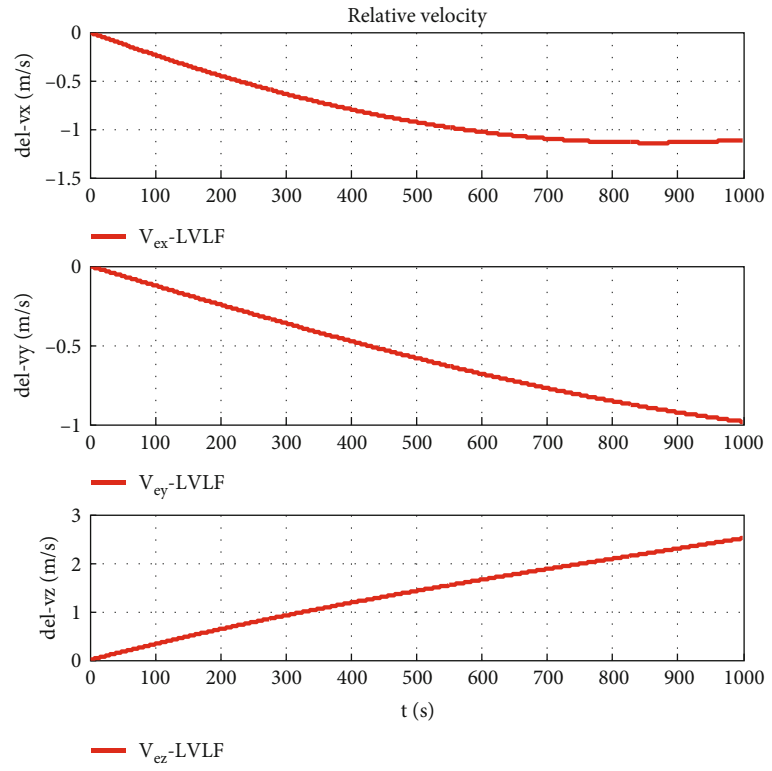

Figure 13: Relative velocity when navigation error is $\Delta\mathbf{r}$.

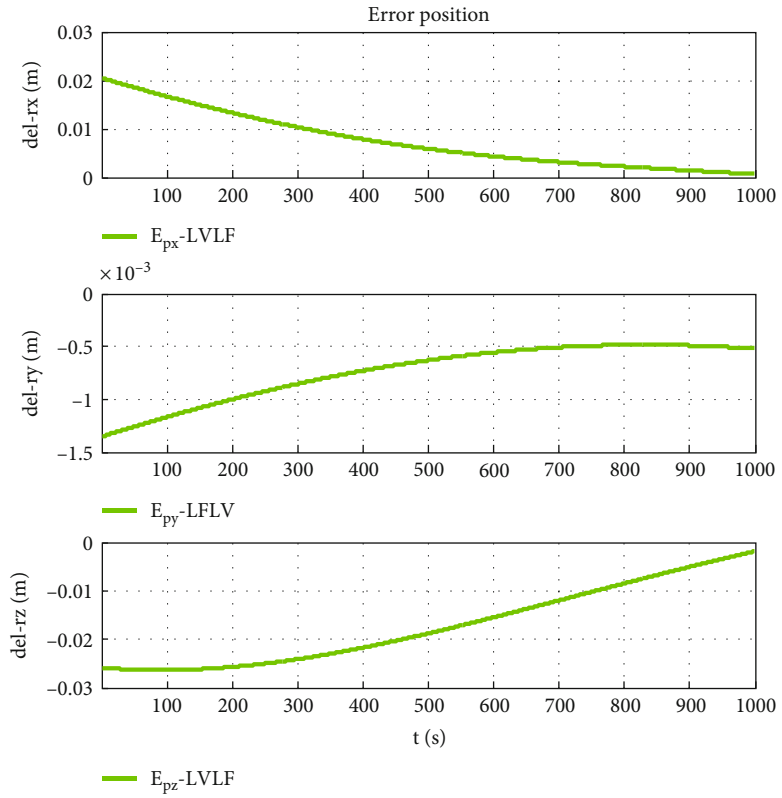

Figure 14: Position errors caused by coordinate conversion.

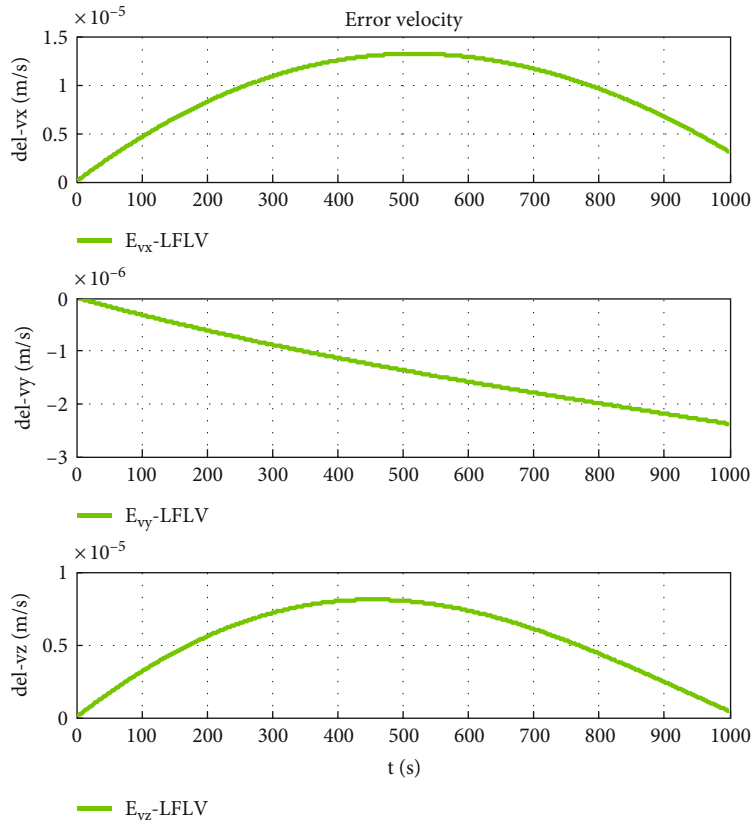

Figure 15: Velocity errors caused by coordinate conversion.

4. Analysis of Engineering Application Advantages

In Section 2, we conclude that attitude-orbit coupling effect between the COMs of spacecraft originates from the selection of reference coordinate system. However, compared with the attitude-orbit-independent relative dynamic equation, the following model advantages of the dual-spinor-based attitude-orbit coupling relative dynamic model can be summarized.

1. In terms of mathematical expression, the dual-spinor-based attitude-orbit coupling relative dynamic model is an integrated representation, which is more concise in mathematical expression and faster in numerical calculation compared to the particle model.

2. In terms of physical phenomenon presentation, the dual-spinor-based attitude-orbit coupling relative dynamic model illustrates the relative motion phenomenon using oneself as an observer.

3. In terms of engineering application, in spacecraft GNC systems, the measured results of currently developed high-precision measurement sensors of relative states, such as high-accuracy metrology sensor based on laser metrology in PROBA-3 mission [32] and optical sensor in multispacecraft formation mission [33], are the relative differentials with respect to the spacecraft body-fixed coordinate system. Therefore, the controller constructed based on the attitude-orbit coupling model achieves higher control accuracy.

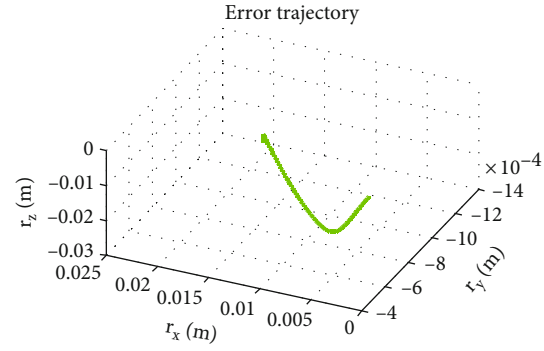

Figure 16: Relative motion trajectory errors caused by coordinate conversion.

5. Simulation and Results

In this section, the advantage of engineering application of the attitude-orbit coupling relative dynamics is verified by numerical simulation. The GNC system of the spacecraft in a spacecraft proximity mission is shown as Figure 5. Taking the measurement sensors (high-accuracy metrology

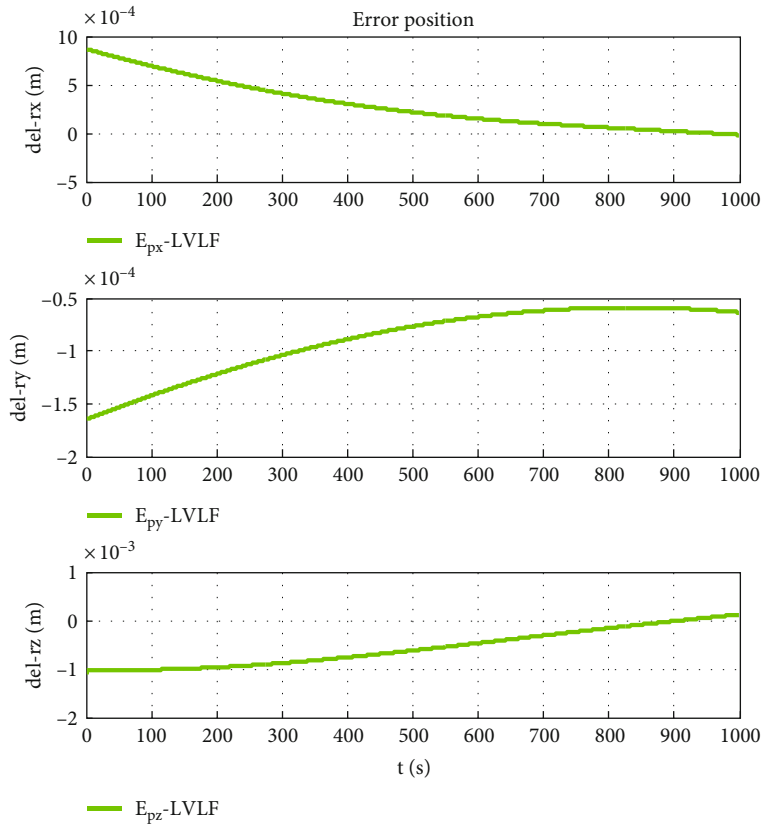

Figure 17: Position errors caused by coordinate conversion when $\Delta\mathbf{r} = 10$ m.

sensor based on laser metrology) of the PROBA-3 mission as an example, measured results are the relative differentials with respect to the spacecraft body-fixed coordinate system of the follower and have 25 μm measurement accuracy, as shown in Figure 6.

In this GNC system, coordinate conversion must be adopted if using attitude-orbit-independent dynamic equation, Equations (1)–(5). In contrast, coordinate conversion is not required if using attitude-orbit coupling dynamic equations, Equations (6), (7), and (37). That is, the main advantage of attitude-orbit coupling dynamic equations in GNC system is reducing errors and computational complexity caused by the coordinate conversion process. In order to quantitatively present the errors caused by the coordinate conversion process, Equations (1) and (37) are selected as an example. Equation (1) is presented with respect to the inertial coordinate system, and the following coordinate conversion process should be adopted if using the GNC system shown in Figure 6.

$$\mathbf{C}_{IB} = \mathbf{C}_{IO} \cdot \mathbf{C}_{OB} \tag{39}$$

where $\mathbf{C}_{IB}$ is the coordinate conversion matrix from the inertial coordinate system to the body-fixed coordinate system, $\mathbf{C}_{IO}$ is the coordinate conversion matrix from the inertial coordinate system to the orbital coordinate system, and $\mathbf{C}_{OB}$ is the coordinate conversion matrix from the orbital coordinate system to the body-fixed coordinate system.

In GNC system, relative dynamic data of Equation (1) need to be converted to the body-fixed coordinate system through Equation (38) to match the relative measurement data. The data of Equation (37) does not require this step. The coordinate conversion matrix $\mathbf{C}_{IO}$ can be expressed as

$$\mathbf{C}_{IO} = \begin{bmatrix} \mathbf{x}_o & \mathbf{y}_o & \mathbf{z}_o \end{bmatrix}^{\mathrm{T}} \tag{40}$$

where $\mathbf{x}_o = \mathbf{y}_o \times \mathbf{z}_o$, $\mathbf{y}_o = (\mathbf{v} \times \mathbf{r})/|\mathbf{v} \times \mathbf{r}|$, and $\mathbf{z}_o = -\mathbf{r}/|\mathbf{r}|$. $\mathbf{r}$ and $\mathbf{v}$ are the position vector and velocity vector of the spacecraft with respect to the inertial system, respectively. In aerospace engineering, $\mathbf{r}$ and $\mathbf{v}$ are related to the orbit determination accuracy of spacecraft. In this paper, the orbit determination error is defined as $\Delta\mathbf{r}$.

Assuming that the leader is deployed in a 500-km circular orbit, its body-fixed coordinate system coincides with the orbital coordinate system. The orbital motion of the leader is governed by gravity ($\mathbf{F}_g = -\mu\mathbf{r}_{AI}/\|r_{AI}\|^3$, $\mu = 398600.44\,\mathrm{km}^3 \times \mathrm{s}^{-2}$), and the influence of other forces and noises is neglected. The mass and moment of inertia of the leader are

$$m_A = 100\mathrm{kg},\ \mathbf{J}_A = \begin{bmatrix} 50 & 0 & 0 \\ 0 & 45 & 0 \\ 0 & 0 & 50 \end{bmatrix} \mathrm{kg} \cdot \mathrm{m}^2.$$

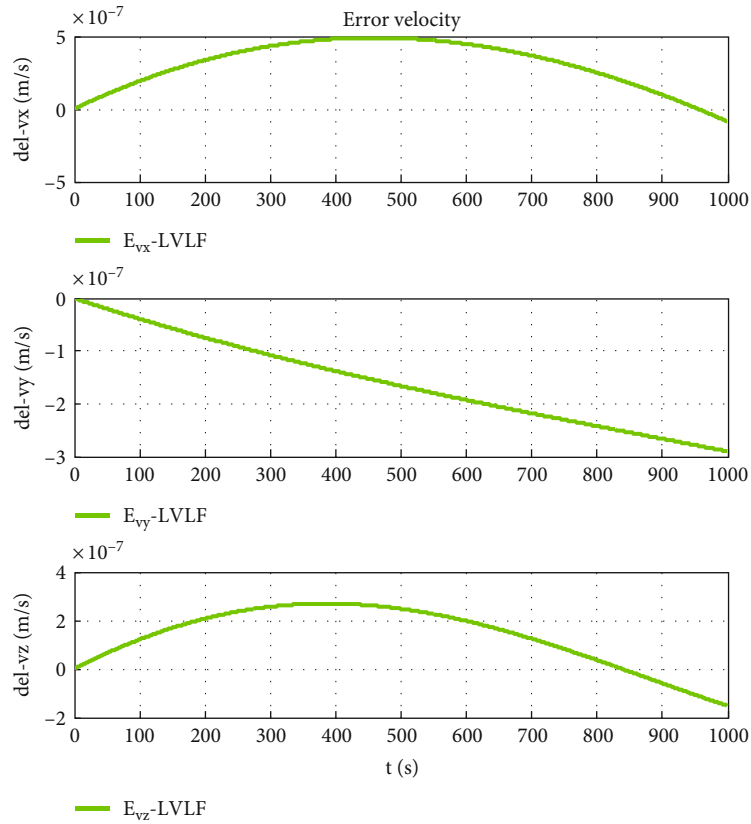

Figure 18: Velocity errors caused by coordinate conversion when $\Delta\mathbf{r} = 10$ m.

The initial position and velocity of the leader with respect to the inertial coordinate system are

$$\mathbf{r}_{IA}^{I}(0) = [5955267 \quad 2431228 \quad 2431228]^{\mathrm{T}}\mathrm{m}, \mathbf{v}_{IA}^{I}(0) = [-3774.2 \quad 4729.1 \quad 4729.1]^{\mathrm{T}}\mathrm{m/s}.$$

The initial attitude quaternion and angular velocity of the leader with respect to the inertial coordinate system are

$$\mathbf{q}_{A}(0) = [0.8924 \quad 0.3696 \quad -0.0990 \quad -0.2391]^{\mathrm{T}}, \boldsymbol{\omega}_{A}^{I}(0) = [0 \quad 0.0011067 \quad 0]^{\mathrm{T}}\mathrm{rad/s}.$$

The mass, moment of inertia, and attitude motion of the follower are the same as those of the leader. The relative position and relative velocity between the follower and the leader with respect to the inertial coordinate system are

$$\mathbf{r}_{fl}^{I}(0) = [2230 \quad 1088 \quad -900]^{\mathrm{T}}\mathrm{m}, \mathbf{v}_{fl}^{I}(0) = [0 \quad 0 \quad 0]^{\mathrm{T}}\mathrm{m/s}.$$

Taking the body-fixed coordinate system of the follower as the conference coordinate system and assuming that the orbit determination accuracy is $\Delta\mathbf{r} = 100$ m, the simulation step length is 0.1 s, and the simulation time is 1000 s, and using the coordinate conversion matrix $\mathbf{C}_{IO}$, the relative motion states are shown in Figures 7–16.

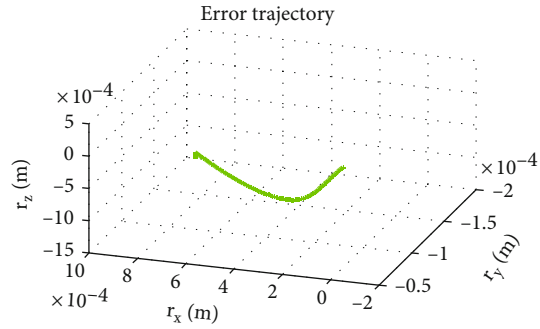

Figure 19: Relative motion trajectory errors caused by coordinate conversion when $\Delta\mathbf{r} = 10$ m.

The orbit determination accuracy is set to $\Delta\mathbf{r} = 10$ m, and other parameters remain unchanged. Simulation results are shown as Figures 17–19.

The orbit determination accuracy is set to $\Delta\mathbf{r} = 1$ m, and other parameters remain unchanged. Simulation results are shown as Figures 20–22.

Figure 7 is the relative trajectory of two spacecraft in the inertial coordinate system, where the red line represents the trajectory of the leader and the blue line

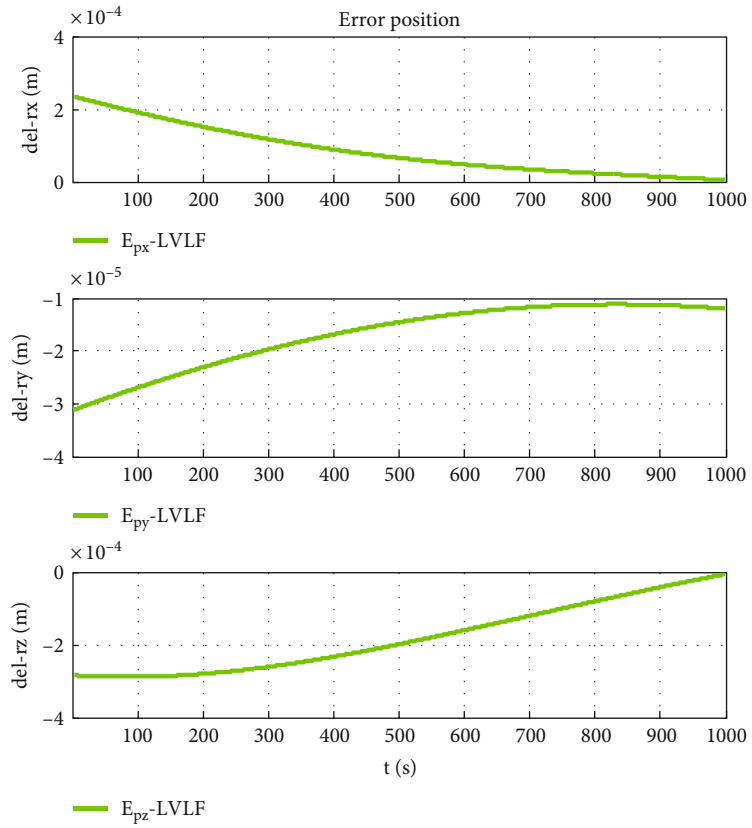

Figure 20: Position errors caused by coordinate conversion when $\Delta\mathbf{r} = 1$ m.

represents the trajectory of the follower. Figures 8 and 9 show the true values of the relative positions and velocities of two spacecraft in the inertial coordinate system, respectively. Figures 10 and 11 show the three-axis relative position curve between two spacecraft in the body-fixed coordinate system of the follower when orbit determination accuracy is zero and $\Delta\mathbf{r}$, respectively. Figures 12 and 13 show the three-axis relative velocity curve between two spacecraft in the body-fixed coordinate system of the follower when orbit determination accuracy is zero and $\Delta\mathbf{r}$, respectively. Figure 14 is the three-axis relative position error between two spacecraft due to coordinate conversion errors with respect to the body-fixed coordinate system of the follower, which is the difference curve between Figures 10 and 11. Figure 15 is the three-axis relative velocity error between two spacecraft due to coordinate conversion errors with respect to the body-fixed coordinate system of the follower, which is the difference curve between Figures 12 and 13. Figure 16 shows the relative motion trajectory error of two spacecraft due to coordinate conversion errors. Figures 17 and 20 is the three-axis relative position error between two spacecraft due to coordinate conversion errors with respect to the body-fixed coordinate system of the follower when $\Delta\mathbf{r} = 10$ m and $\Delta\mathbf{r} = 1$ m, respectively. Figures 18 and 21 is the three-axis relative velocity error between two spacecraft due to coordinate conversion errors with respect to the body-fixed coordinate system of the follower when $\Delta\mathbf{r} = 10$ m and $\Delta\mathbf{r} = 1$ m, respectively. Figures 19 and 22 show the relative motion trajectory error of two spacecraft due to coordinate conversion errors when $\Delta\mathbf{r} = 10$ m and $\Delta\mathbf{r} = 1$ m, respectively.

From Figure 14, we can conclude that when the orbit determination error is 100 m, the relative position description error caused by coordinate conversion errors is about 0.03 m, which indicates that, even if the relative data obtained by spacecraft using relative measurement sensors are absolutely accurate, the error caused by coordinate rotation can reach 0.03 m. This error even exceeds the measurement error of the sensor (25 μm). According to Figures 12, 13, and 15, the relative velocity description error caused by coordinate conversion error is about 0.015 mm/s. From Figures 14, 17, and 20, we found that the higher the orbit determination accuracy, the smaller the error caused by coordinate conversion, but it is still greater than the measurement error of the relative measurement sensor. From Figures 7–16, it can be seen that within 1000 s, the relative motion error between spacecraft caused by coordinate conversion increases as a whole over time. Considering the high efficiency characteristics of precision collaborative tasks such as precision spacecraft formation flying, the one-time working time of the spacecraft will not be too long. Therefore, the simulation duration of 1000 s is within a reasonable range, resulting in a relative motion description error of about

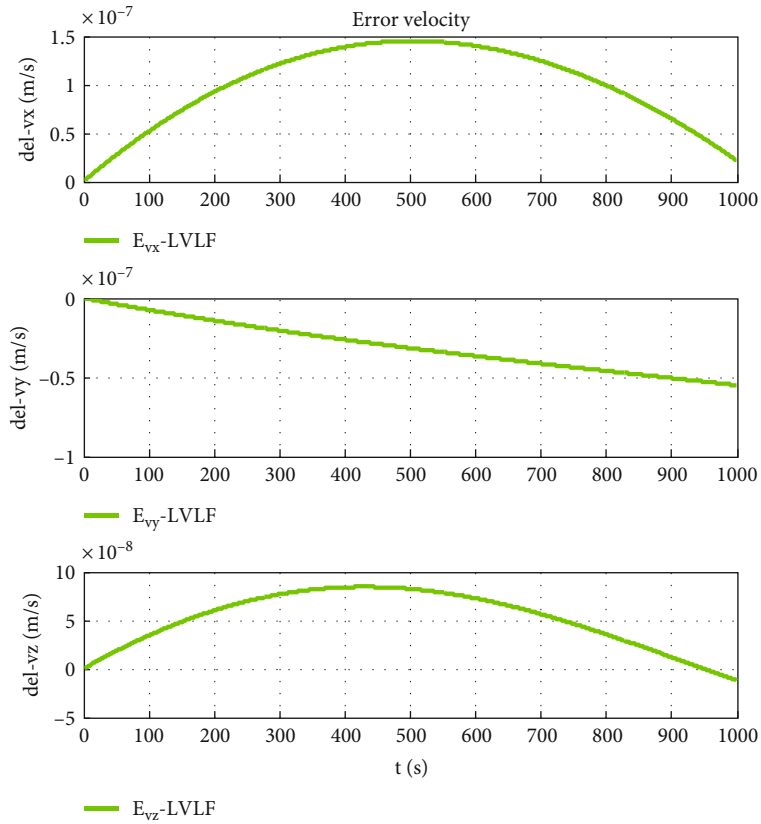

Figure 21: Velocity errors caused by coordinate conversion when $\Delta\mathbf{r} = 1$ m.

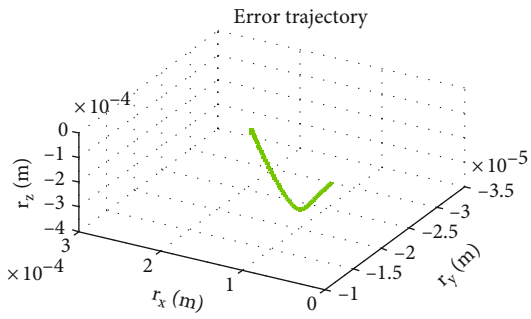

Figure 22: Relative motion trajectory errors caused by coordinate conversion when $\Delta\mathbf{r} = 1$ m.

centimeters, which basically exceeds the indicator requirements for precision collaborative tasks such as precision spacecraft formation flying.

6. Conclusions

This article mainly completes two innovative contents. First, through the study of attitude-orbit coupling dynamic mechanism and mathematical representation, we conclude that one of the main root causes of attitude-orbit coupling effects of spacecraft proximity relative motion is the selection of the reference coordinate system. Second, through extending the representation of dual spinors to flexible body, the attitude-orbit coupling dynamic model between a rigid-flexible coupling spacecraft and a rigid spacecraft is developed. Based on the above analysis and modeling work, the engineering application advantages of the attitude-orbit coupling relative dynamics is provided. Simulation results show that in GNC systems for precision collaborative missions, the use of attitude-orbit coupling relative dynamic model can reduce the errors and computational complexity caused by coordinate conversion. Our next work is aimed at investigating control methods based on attitude-orbit coupling dynamics, like model predictive control method [34] linear matrix inequality approach [9], and other control method [35–37].

Data Availability Statement

The data used to support the findings of this study are included within this paper.

Conflicts of Interest

The authors declare no conflicts of interest.

Funding

This research was supported by the Fundamental Research Funds for the Central Universities of China (No. 307202 2JC0202), the project D030307.

References

[1] G. Misra, M. Izadi, A. Sanyal, and D. Scheeres, "Coupled orbit–attitude dynamics and relative state estimation of spacecraft near small solar system bodies," *Advances in Space Research*, vol. 57, no. 8, pp. 1747–1761, 2016.

[2] A. Chaves-Jiménez, J. Guo, and E. Gill, "Impact of atmospheric coupling between orbit and attitude in relative dynamics observability," *Journal of Guidance, Control, and Dynamics*, vol. 40, no. 12, pp. 3274–3281, 2017.

[3] A. Chaves-Jiménez, J. Guo, and E. Gill, "Impact of dynamic coupling between relative orbit and attitude on the estimation of relative dynamics of spacecraft," *Acta Astronautica*, vol. 152, pp. 850–858, 2018.

[4] B. McCann and M. Nazari, "Analysis of the impact of orbit-attitude coupling at higher-degree potential models on spacecraft dynamics," *The Journal of the Astronautical Sciences*, vol. 69, no. 4, pp. 955–987, 2022.

[5] Y. Liu, S. Wu, K. Zhang, and Z. Wu, "Gravitational orbit–attitude coupling dynamics of a large solar power satellite," *Aerospace Science and Technology*, vol. 62, pp. 46–54, 2017.

[6] H. Zhang, J. Li, Z. Wang, and Y. Guan, "Guidance navigation and control for chang'E-5 powered descent," *Space: Science & Technology*, vol. 2021, Article ID 9823609, 2021.

[7] L. Chen, X. Fu, S. Ramil, and M. Xu, "Intelligent fuzzy control in stabilizing solar sail with individually controllable elements," *Space: Science & Technology*, vol. 2022, Article ID 9831270, 2022.

[8] K. Shi, C. Liu, Z. Sun, and X. Yue, "Coupled orbit-attitude dynamics and trajectory tracking control for spacecraft electromagnetic docking," *Applied Mathematical Modelling*, vol. 101, pp. 553–572, 2022.

[9] C. Liu, X. Yue, K. Shi, and Z. Sun, *Spacecraft Attitude Control: A Linear Matrix Inequality Approach*, Elsevier, Amsterdam, 2022.

[10] W. H. Clohessy and R. S. Wiltshire, "Terminal guidance system for satellite rendezvous," *Journal of the Aerospace Sciences*, vol. 27, no. 9, pp. 653–658, 1960.

[11] T. M. Davis and D. Melanson, "XSS-10 microsatellite flight demonstration program results," in *Proceedings of the Spacecraft Platforms and Infrastructure Conference, SPIE-The International Society for Optics and Photonics*, pp. 16–25, Bellingham, USA, 2004.

[12] J. Sullivan, S. Grimberg, and S. D'Amico, "Comprehensive survey and assessment of spacecraft relative motion dynamics models," *Journal of Guidance, Control, and Dynamics*, vol. 40, no. 8, pp. 1837–1859, 2017.

[13] X. Zhang, W. Zhu, Y. Xie, X. Wu, and J. Guo, "Cross-coupling relative dynamics for on-orbit assembly in rotating frame of reference," *Applied Mathematical Modelling*, vol. 116, pp. 372–392, 2023.

[14] Y. Wu, X. Hu, D. Hu, T. Li, and J. Lian, "Strapdown inertial navigation system algorithms based on dual quaternions," *IEEE Transactions on Aerospace and Electronic Systems*, vol. 41, no. 1, pp. 110–132, 2005.

[15] D. Gan, Q. Liao, S. Wei, J. S. Dai, and S. Qiao, "Dual quaternion-based inverse kinematics of the general spatial 7R mechanism," *Proceedings of the Institution of Mechanical Engineers, Part C: Journal of Mechanical Engineering Science*, vol. 222, no. 8, pp. 1593–1598, 2008.

[16] A. Perez and J. McCarthy, "Dual quaternion synthesis of constrained robotic systems," *Journal of Mechanical Design*, vol. 126, no. 3, pp. 425–435, 2004.

[17] V. Kapila, A. Sparks, J. Buffington, and Q. Yan, "Spacecraft formation flying: dynamics and control," in *Proceedings of American Control Conference*, San Diego, USA, 1999.

[18] Z. Zhang and J. Li, "Orbit and attitude control of spacecraft formation flying," *Applied Mathematics and Mechanics*, vol. 29, no. 1, pp. 43–50, 2008.

[19] T. Chen, J. Shan, and H. Wen, *Distributed Attitude Consensus of Multiple Flexible Spacecraft*, 2023, *Springer Singapore*.

[20] T. Chen, J. Shan, H. Wen, and S. Xu, "Review of attitude consensus of multiple spacecraft," *Astrodynamics*, vol. 6, no. 4, pp. 329–356, 2022.

[21] T. Chen and J. Shan, "Distributed spacecraft attitude tracking and synchronization under directed graphs," *Aerospace Science and Technology*, vol. 109, article 106432, 2021.

[22] J. Chamberlin and J. Rose, "Gemini rendezvous program," *Journal of Spacecraft and Rockets*, vol. 1, no. 1, pp. 13–18, 1964.

[23] J. Goodman, "History of space shuttle rendezvous and proximity operations," *Journal of Spacecraft and Rockets*, vol. 43, no. 5, pp. 944–959, 2006.

[24] I. Kawano, M. Mokuno, T. Kasai, and T. Suzuki, "First autonomous rendezvous using relative GPS navigation by ETS-VII," *Navigation*, vol. 48, no. 1, pp. 49–56, 2001.

[25] S. Segal and P. Gurfil, "Effect of kinematic rotation-translation coupling on relative spacecraft translational dynamics," *Journal of Guidance, Control, and Dynamics*, vol. 32, no. 3, pp. 1045–1050, 2009.

[26] H. Pan and V. Kapila, "Adaptive nonlinear control for spacecraft formation flying with coupled translational and attitude dynamics," in *Proceedings of the 40th IEEE Conference on Decision and Control (Cat. No.01CH37228)*, vol. 3, pp. 2057–2062, Orlando, FL, USA, 2001.

[27] J. Sun, X. Zhang, X. Wu, and T. Song, "Dual-quaternion-based translation-rotation-vibration integrated dynamics modeling for flexible spacecraft," *Journal of Aerospace Engineering*, vol. 32, no. 1, article 04018135, 2019.

[28] X. Zhang, W. Zhu, X. Wu, T. Song, Y. Xie, and H. Zhao, "Dynamics and control for in-space assembly robots with large translational and rotational maneuvers," *Acta Astronautica*, vol. 174, pp. 166–179, 2020.

[29] Y. Xie, X. Zhang, X. Song, X. Lian, and J. Zhang, "Integrated dynamics of space rigid-flex combination system with time-varying configuration," *International Journal of Aerospace Engineering*, vol. 2023, Article ID 9980780, 16 pages, 2023.

[30] H. Du, M. Chen, and G. Wen, "Leader–following attitude consensus for spacecraft formation with rigid and flexible spacecraft," *Journal of Guidance, Control, and Dynamics*, vol. 39, no. 4, pp. 944–951, 2016.

[31] L. Felicetti and M. Emami, "A multi-spacecraft formation approach to space debris surveillance," *Acta Astronautica*, vol. 127, pp. 491–504, 2016.

[32] J. Llorente, A. Agenjo, C. Carrascosa et al., "PROBA-3: precise formation flying demonstration mission," *Acta Astronautica*, vol. 82, no. 1, pp. 38–46, 2013.

[33] V. Brodsky and M. Shoham, "Dual numbers representation of rigid body dynamics," *Mechanism and Machine Theory*, vol. 34, no. 5, pp. 693–718, 1999.

[34] L. Ge, J. Guo, S. Mao et al., "A composite model predictive control method of SRMs with PWM-based signal for torque ripple

suppression," *IEEE Transactions on Transportation Electrification*, 2024.

[35] Q. Meng, M. Huang, Y. Xu, N. Liu, and X. Xiang, "Decentralized distributed deep learning with low-bandwidth consumption for smart constellations," *Space: Science & Technology*, vol. 2021, Article ID 9879246, 2021.

[36] G. Blossey, "A stochastic modeling approach for interplanetary supply chain planning," *Space: Science & Technology*, vol. 3, p. 0014, 2023.

[37] J. Tayebi, T. Chen, and H. Wang, "Dynamics and control of flexible satellite using reaction sphere actuators," *Space: Science & Technology*, vol. 3, 2023.